2017

Substrate Integrated E-plane Horn Antenna and Antenna Array

Zhewei Gu
Minnesota State University, Mankato

Substrate Integrated E-plane Horn Antenna and Antenna Array

By

Zhewei Gu

A Thesis Submitted in Partial fulfillment of the

Requirements for the degree of

Master of Science

in

Electrical and Computer Engineering Technology

Minnesota State University, Mankato

Mankato, Minnesota

05/2017

Date: **04/07/2017**

Title: **Substrate Integrated E-plane Horn Antenna and Antenna Array**

Student's Name: **Zhewei Gu**

This thesis has been examined and approved by the following members of the student's committee.

_____

Dr. Xuanhui Wu Advisor

_____

Dr. Khaliq Muhammad Committee Member

_____

Dr. Qun Zhang Committee Member

Declaration of Authorship

I, Zhewei GU, declare that this thesis titled, "Substrate Integrated E-plane Horn Antenna and Antenna Array" and the work presented in it are my own. I confirm that:

- This work was done wholly or mainly while in candidature for a research degree at this University.
- Where any part of this thesis has previously been submitted for a degree or any other qualification at this University or any other institution, this has been clearly stated.
- Where I have consulted the published work of others, this is always clearly attributed.
- Where I have quoted from the work of others, the source is always given. With the exception of such quotations, this thesis is entirely my own work.
- I have acknowledged all main sources of help.
- Where the thesis is based on work done by myself jointly with others, I have made clear exactly what was done by others and what I have contributed myself.

Signed: Zhewei Gu

Date: 04/07/2017

MINNESOTA STATE UNIVERSITY, MANKATO

2017

Abstract

Electrical and Computer Engineering Technology

Master of Science

Substrate Integrated E-plane Horn Antenna and Antenna Array

by Zhewei Gu

In this paper, a novel SMA fed substrate integrated E-plane horn antenna and antenna array are proposed. The substrate integrated E-plane waveguide (SIEW) is not only able to integrate conventional waveguide circuits on printed circuit boards (PCB), but also especially falls into all E-plane circuits which substrate integrated waveguide (SIW) technique fails to. Essential copper strips are sandwiched in the middle by two PCBs to support longitudinal current in the E-plane fed through an SIEW-to-SMA transition. Copper plated holes aligned along the wave propagation direction are drilled through the substrate and copper strips, so that vertical current in the H-plane can also be supported. In order to minimize the reflections due to discontinuity between substrate and the free space, a dielectric load is placed in front of the aperture for lower return loss and better gain performance. Moreover, a two-element antenna array fed through a Y-junction power divider is also designed and prototyped for further performance enhancement. Good agreement between results from simulation and measurement is achieved.

Acknowledgements

First of all, I would like to sincerely thank my advisor, Dr. Xuanhui Wu, for his mentoring through all these three years. More than an academic advisor, he is also a close friend of mine, who cares and motivates me in my life. Without his continuous and patient guidance on my reserch projects, I would have never been able to accomplish this work.

I also would like to thank my commmittee members, Dr. Qun Zhang and Dr. Muhammad Khaliq, for their help and encouragement. They also gave me so many advices along the way in my master's study and motivations in pursuing further Ph.D. study.

Finally, I would like to thank my families for their endless love and support without expecting for return. Without their encouragement, I would not have accomplished all these.

Contents

List of Figures

List of Abbreviations

RF	**R**adio **F**requency
AC	**A**lternating **C**urrent
TEM	**T**ransverse **E**lectric **M**agnetic
TE	**T**ransverse **E**lectric
TM	**T**ransverse **M**agnetic
SIW	**S**ubstrate **I**ntegrated **W**aveguide
PCB	**P**rinted **C**ircuit **B**oard
SIEW	**S**ubstrate **I**ntegrated **E**plane **W**aveguide
Co-pol	**C**o - **P**olarization
X-pol	**C**ross - **P**olarization

Dedicated to my family

1 Introduction

1.1 Conventional Waveguide Circuit

Transmission line is a type of cable or structure that is used in high-frequency applications, such as RF and microwave circuits, to transmit alternating current (AC). Since the frequency of such current is very high, the behaviour of the transmission line will be quite diffrent from the low-frequency transmission medium and the wave nature has to be taken into account. There are several commonly used transmission lines shown in Fig. 1.1 - Fig. 1.4, including coaxial lines, microstrip lines, two wire lines and waveguides.

Among aforementioned transmission lines, waveguide, as shown in Fig. 1.4, has outstanding performances. The basic structure of a waveguide is a hollow pipe with metallic walls and is filled up with air or other substrate in the cavity. Unlike other aforementioned transimission lines which can support transverse electric magnetic (TEM) mode, only transverse electric (TE) mode and transverse magnetic (TM) mode can exist in a waveguide. The reanson is explained in [1]. In brief, if both the electric and magnetic components are transverse to the wave propagation direction, the wave is unable to propagate along this direction. Generally speaking, the conventional waveguide circuit has two typical structures with the fixed height as shown in Fig. 1.5. The left structure is called E-plane circuit where the electric field is horizontally polarized. The other one is called H-plane circuit where the magnetic field is horizontally polarized and parallel to the ground plane. In both circuits, it is assumed that only the fundamental mode is excited so that the electric field is always pointing from the long wall of the waveguide circuit to the other. The enerygy can be well sustained during transmission since metallic walls of the circuit can well restrict the energy in the cavity [1], [2]. Besides,

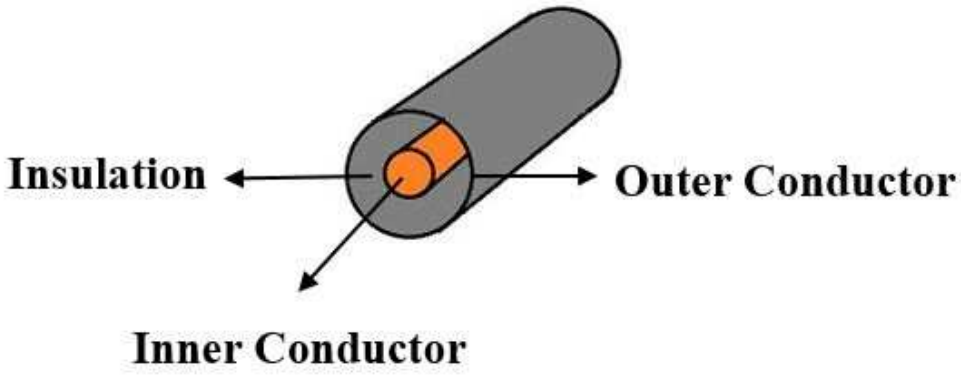

FIGURE 1.1: Coaxial line model

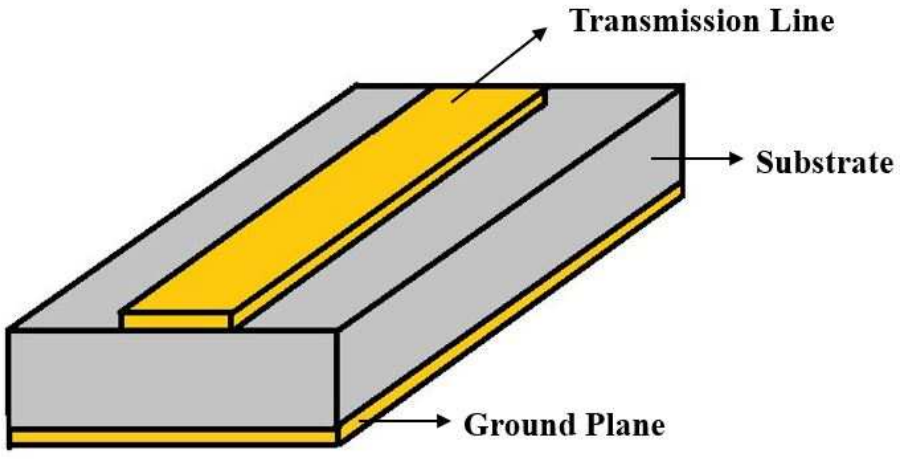

FIGURE 1.2: Microstrip line model

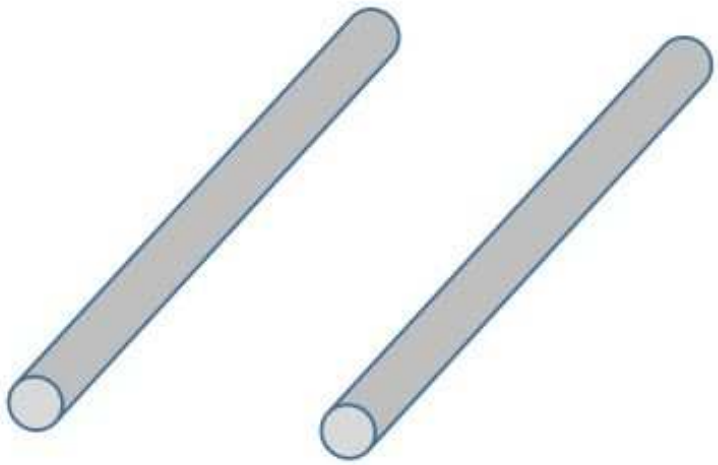

FIGURE 1.3: Two-wire line model

it also has some other advantages, including high power capacity and high Q-factor [3]- [5]. Thanks to all these advantages, conventional waveguide circuit is widely used in many applications since its invention, such as antennas [6]- [8], filters [9]- [11], couplers [12] [13] and diplexers [14] [15]. However, the deficiencies of conventional waveguide circuits are also obvious. Their structures are usually very bulky, which limits their applications especially in compact circuit designs. Moreover, due to being made of metallic matrial, the fabrications are always time- and cost-consuming, which limits the their capability of miassive production.

1.2 Substrate Integrated Waveguide (SIW) Technique

As the development of integrated circuit industry, reserchers and engineers were trying to overcome the deficiencies of conventional waveguide circuits while still

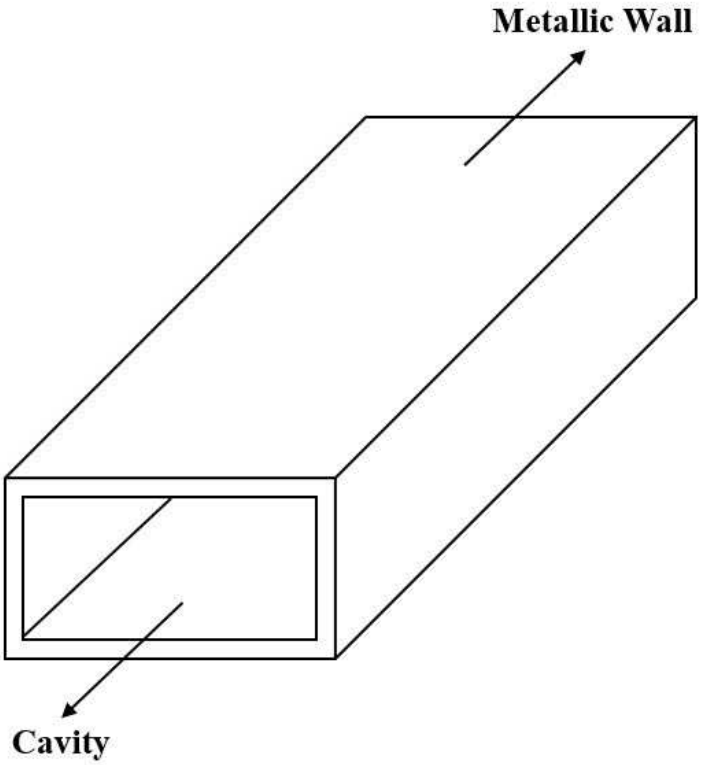

FIGURE 1.4: Metallic rectangular waveguide model

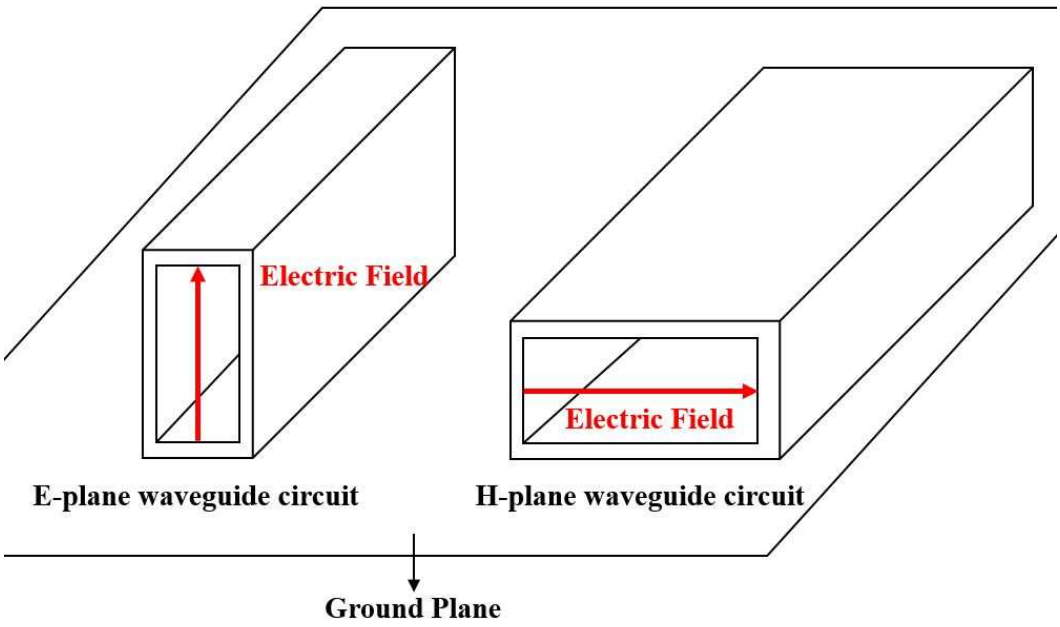

FIGURE 1.5: Two basic types of waveguide circuits

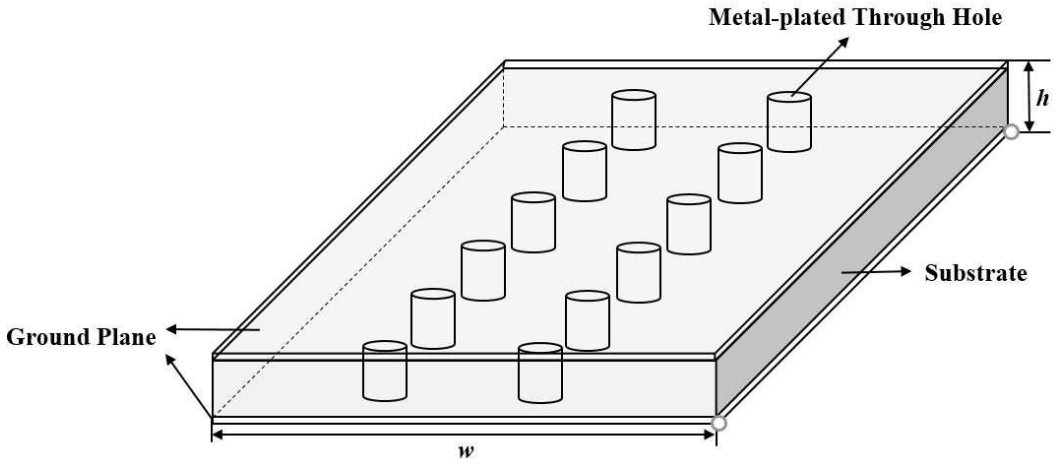

FIGURE 1.6: Basic structure of SIW circuit

keeing their good characteristics. In the process of tackling aforementioned deficiencies, a new type of waveguide circuit was developed with the help of multilayer processing technique, which is called substrate integrated waveguide (SIW). This concept was firstly demonstarted in [16]. The SIW technique is able to integrate a planar waveguides on a piece of printed circuit board (PCB). As we know, the typical PCB has two metal-plated surfaces, both of which can be utilized to emulate the top and bottom walls of a waveguide to support both horizontal can longitudinal current based on the boundary condition $\hat{n} \times \vec{H} = \vec{J}_s$. Additionally, as shown in Fig. 1.6, some metal-plated holes are drilled through the PCB. Based on the principles presented in [17] and [18], if the parameters in Fig. 1.7 are well designed and optimized, the energy leakage can be sufficientlly minimized. In another words, these metal-plated through holes can be utilized to emulate the lateral walls of a waveguide. These conclusions can also be validated from both theory can simulations [19].

As shown in Fig. 1.8, an H-plane circuit which is placed in the $x-y$ plane and the electric field is purly polarized in the z-directon under the fundamental TE_{10}

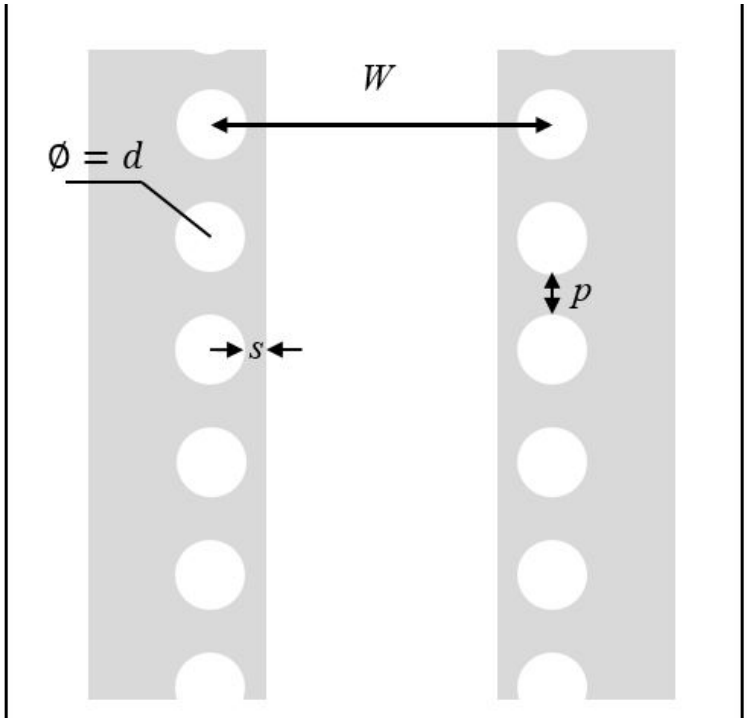

FIGURE 1.7: Cross-view of a section of an SIW circuit

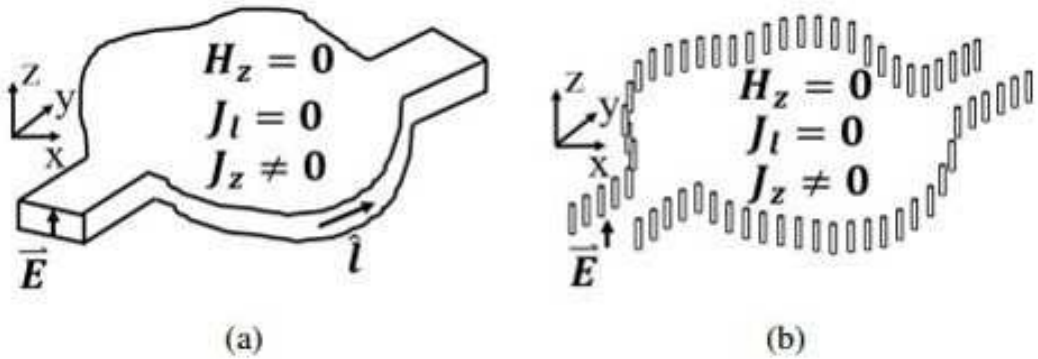

FIGURE 1.8: H-plane waveguide circuit and its SIW implementation. Reprinted from X. H. Wu, D. Huang and Q. Zhang, "Planar Substrate Integrated E-plane Waveguide (SIEW) Circuits", *IEEE Transactions on Microwave Theory and Techniques*, submitted in Apr, 2017.

mode. Since the height of the circuit is fixed without any variations, the electric field in both x and y directions can be considered as zero, namely, $E_x = E_y = 0$. Apply this circumstance on the curl equation of the Maxwell equation

$$\nabla \times \vec{E} = -j\omega\mu\vec{H} \tag{1.1}$$

It will lead to the vertical magnetic field, H_z, to be zero. Furthermore, if the boudary condition $\vec{J} = \hat{n} \times \vec{H}$ is applied on the lateral walls of the circuit, it is can be derived that $J_l = H_z = 0$. Namely, in an H-plane SIW circuit, only the vertical current, rather than the longitudinal current, exists on the lateral walls. This current can be fully guided by those metal-plated through holes. Simulation result is investigated and depicted in Fig. 1.9 [20], from which it reveals the wave is well guided by the circuit along the propagation direction. This new technique has given rise to many applications since its invention, which includes different H-plane circuits, such as SIW waveguide [21]- [23], filters [24]- [26], couplers [27] [28], diplexers [29] [30] and antennas [31]- [20]. From all the researches mentioned above, it has been validated that the SIW technique can successfully implement conventional waveguide circuit while keeping its advantages. Moreover, fabrication costs are hugely reduced by using PCBs to substitute metallic materials.

1.3 Substrate Integrated E-plane Waveguide (SIEW) Technique

As aforementioned, the developed SIW technique can successfully implement H-plane waveguide circuits, however, failures will occur when it tends to implement E-plane waveguide circuits. The basic structure of an E-plane waveguide and the plot of the amplitude of simulated field distribution in the fundamental mode [34] are presented in Fig. 1.10, where the height, h, of lateral walls is larger than the width, w, of top and bottom walls. From the simulation result, it is obvious

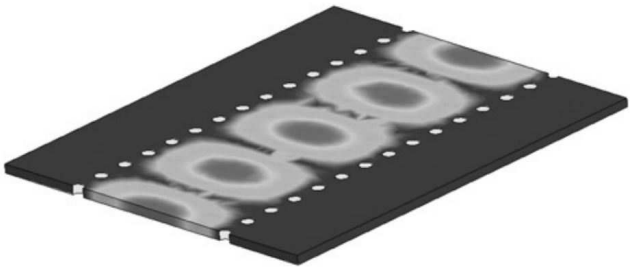

FIGURE 1.9: Plot of amplitude of electric field distribution in an SIW circuit in the fundamental mode. Reprinted from M. Bozzi, A. Georgiadis, and K. Wu, "Review of substrate-integrated waveguide circuits and antennas", *IET Microwaves, Antennas and Propagation*, vol. 5, no. 8, pp. 909-920, 2011.

that, instead of being guided along the wave propagation direction, the wave leaks between metal-plated through holes. The theoretical explanation will be demonstrated as follows [19].

As shown in Fig. 1.11, an equivalent E-plane waveguide circuit is depicted, which is placed in the $x-y$ plane. Consider that in this circuit, only the fundamental mode is desirable to be excited where the electric field is horizontally polarized, namely in the x direction. The electric field existing in the circuit can be expressed as

$$\vec{E}(x,y,z) = [\hat{x}E_x(x,y) + \hat{y}E_y(x,y)]sin(k_z z) \tag{1.2}$$

where $k_z = \frac{\pi}{h}$ with h representing the thickness of the circuit. Substituting eq. 1.2 into eq. 1.1 gives the magnetic field as

$$\begin{aligned}\vec{H}(x,y,z) =& \frac{j}{\omega\mu}\{-\hat{x}k_z E_y(x,y)cos(k_z z) \\ &+\hat{y}k_z E_x(x,y)cos(k_z z) \\ &+\hat{z}sin(k_z z)[\frac{\partial}{\partial x}E_y(x,y) - \frac{\partial}{\partial y}E_x(x,y)]\Big\}\end{aligned} \tag{1.3}$$

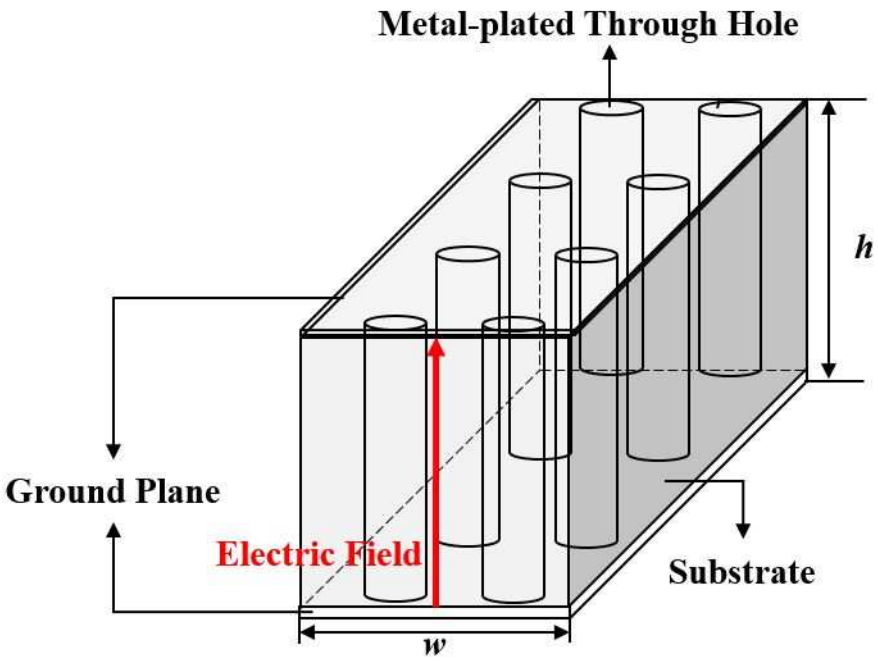

(a)

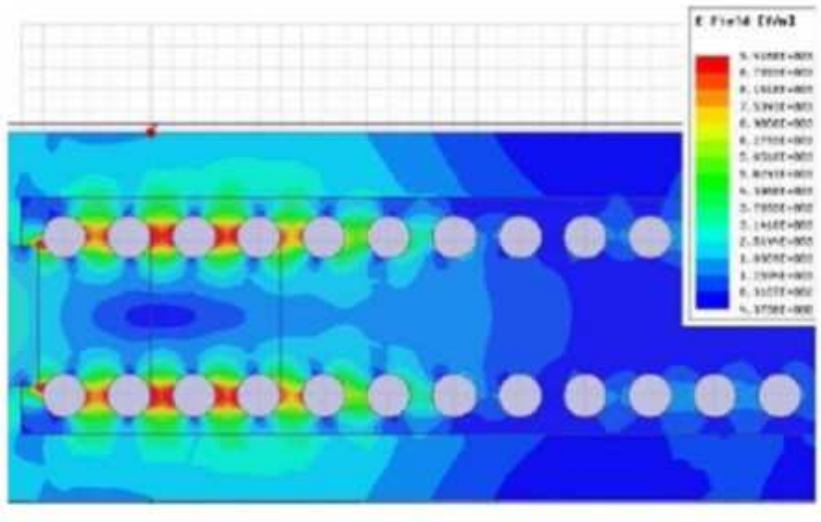

(b)

FIGURE 1.10: (a) General E-plane SIW circuit, (b) Cross-view plot of the amplitude of the electric field distribution of an E-plane SIW circuit in fundamental mode. Reprinted (b) from "Concept of Substrate Integrated E-plane Waveguide and Waveguide Filter" by D. Huang, X. H. Wu and Q. Zhang, *International Workshop on Antenna Technology: Small Antennas, Innovative Structures, and Applications*, Cocoa Beach, FL, USA, Feb. 29 - Mar. 2, 2016.

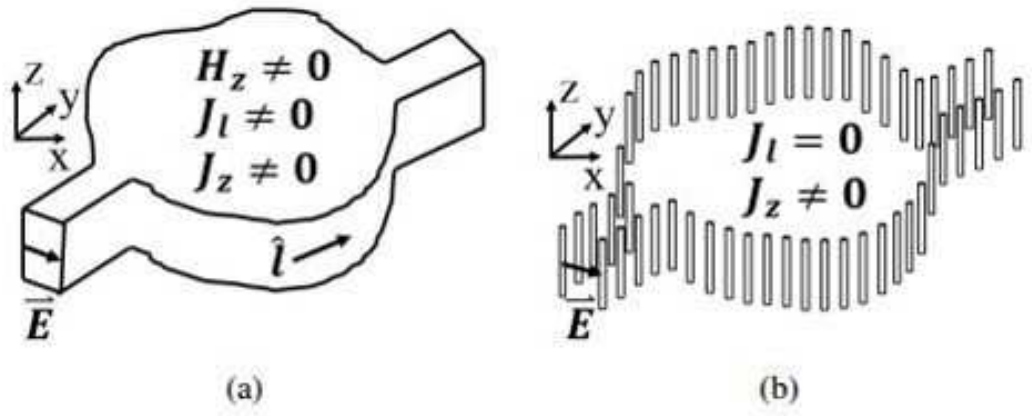

FIGURE 1.11: E-plane waveguide circuit and its SIW implementation. Reprinted from X. H. Wu, D. Huang and Q. Zhang, "Planar Substrate Integrated E-plane Waveguide (SIEW) Circuits", *IEEE Transactions on Microwave Theory and Techniques*, submitted in Apr, 2017.

Consequently, the magnetic field distribution reveals that both vertical current and longitudinal current exist on the lateral walls of the circuit, which are respectively expressed as

$$J_l = \frac{j}{\omega\mu} sin(k_z z)[\frac{\partial}{\partial x} E_y(x,y) - \frac{\partial}{\partial y} E_x(x,y)] \tag{1.4}$$

$$J_z = \frac{jk_z cos(k_z z)}{\omega\mu} [\hat{x} E_y(x,y) - \hat{y} E_x(x,y)] \cdot \hat{l} \tag{1.5}$$

where $\hat{l}$ is the unite vector in the longitudinal direction on the lateral walls. Conclusively, in an E-plane circuit, not only the vertical current, but also the longitudinal current exists. However, in an E-plane SIW circuit, although the vertical current J_z in eq. 1.5 can be fully guided by metal-plated through holes, there is no such a physical structure can be used to support the longitudinal current J_l in eq. 1.4. This is the reason of the occurrence of the failures. Even though some studies applied the SIW technique to implement E-plane circuits by modifying the structure of device, however, requirements are very rigorous and performances are hardly guaranteed. For example, rows of air-holes are drilled beyond metal

plated through holes to decrease the total dielectric constant of the substrate, so that a barrier is formed consequently. Such a barrier can prevent energy leakage. However, the size of circuit will be enlarged thereupon by adding extra rows of air-holes. As sacrifice, the bandwidth of antenna will be narrowed due to the use of high dielectric constant substrate. Conclusively, the SIW technique is inadequate for E-plane circuits unless the physical structure for guiding essential longitudinal current is added.

For the sake of overcoming this issue, the author developed existing SIW technique by introducing additional metal strips as shown in Fig. 1.12(a). These metal strips are sandwiched by two printed circuit boards from the top and bottom sides. Meanwhile, all copper plated through holes remain to guide vertical current. Simulation results are carried out to validate the feasibility of this structure as plotted in Fig. 1.12(b) [34]. From the simulation result, it can be clearly seen that the wave in E-plane is perfectly guided by this new structure. This fire-new concept was firstly demonstrated in [34], and is referred to as substrate integrated E-plane waveguide (SIEW). SIEW technique can be perfectly applied to design both E-plane and H-plane types of integrated circuits. Based on this new technique, several designs have been accomplished, such as SIEW waveguide and filter, which are detailly presented in [34]. In following sections of this dissertation, an SIEW sectorial horn antenna and antenna array whose working frequency band are from 17-19GHz will be proposed. The primary model of this SIEW horn antenna was presented by the author in [35] only with the simulated results. After further researches done by the author, the antenna model has been developed with changing the material of substrate and optimizing the dimensions. Both the single-element antenna and antenna array were fabricated by the author. Better performances have been validated by both simulated and measured results

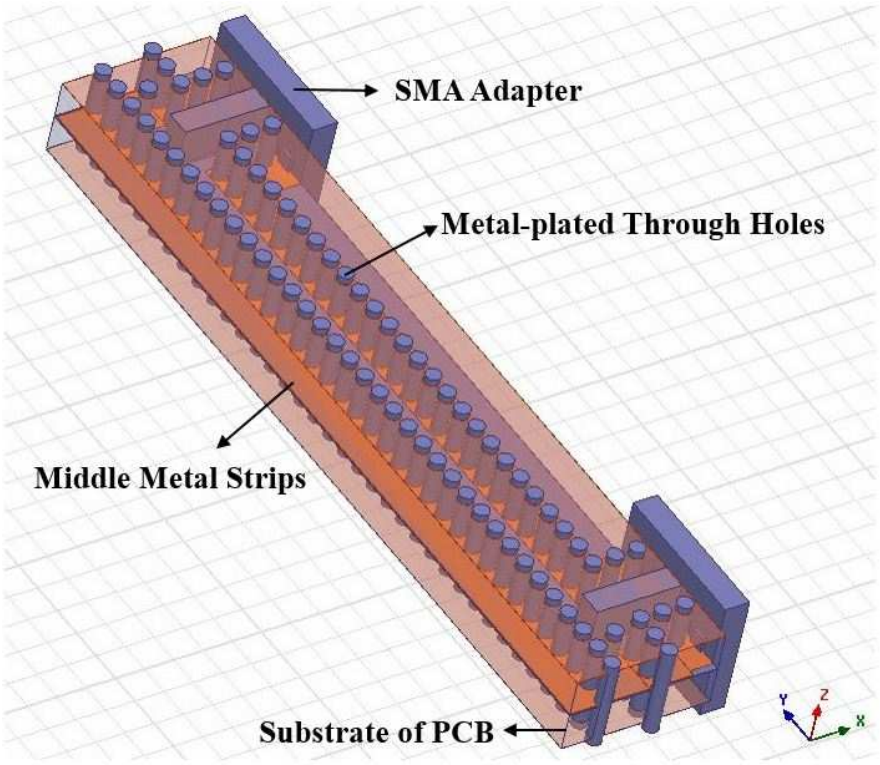

(a)

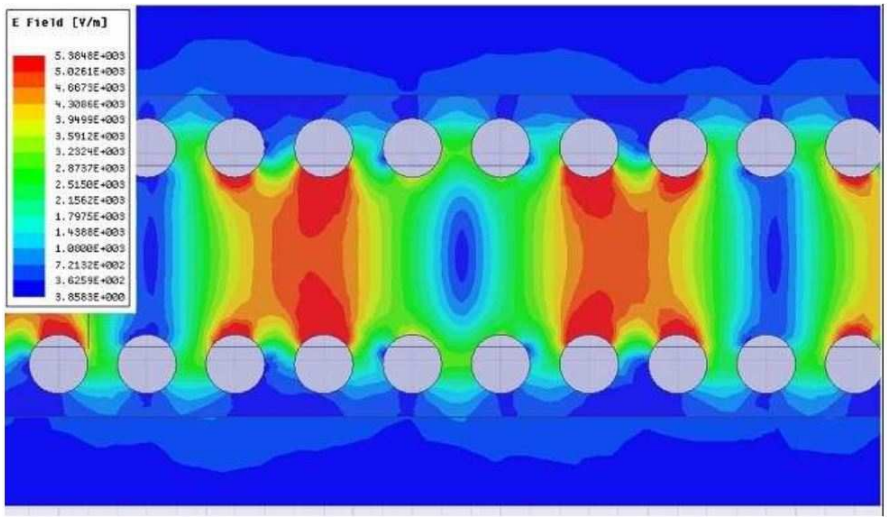

(b)

FIGURE 1.12: (a) 3D structure of substrate integrated E-plane waveguide circuit, (b) Cross-section view of the electric field distribution in an SIEW circuit. Reprinted (a) and (b) from "Concept of Substrate Integrated E-plane Waveguide and Waveguide Filter" by D. Huang, X. H. Wu and Q. Zhang, *International Workshop on Antenna Technology: Small Antennas, Innovative Structures, and Applications*, Cocoa Beach, FL, USA, Feb. 29 - Mar. 2, 2016.

of performances, which will be presented in following sections.

The rest of dissertation is organized as follows. In Chapter 2, the structure and geometry of the single-element SIEW horn antenna is presented. Furthermore, results of simulation and measurement, as well as parametric studies of the dielectric load and SIEW-to-SMA transition are also presented and analyzed. In Chapter 3, the SIEW horn antenna array is proposed with presenting its transmitting and radiating performances. The further study of the quarter-wavelength impedance transformer embedded between the power divider and horn antennas is also presented in this section. All simulation results and performance evaluations were carried out by the full wave solver, Ansoft HFSS. This dissertation is concluded in Chapter 4.

2 Single-element SIEW Sectorial Horn Antenna

2.1 Antenna Geometry

The geometry of single-element SIEW horn antenna is depicted in Fig. 2.1. The whole circuit consists of an SIEW-to-SMA transition, a horn section and a trapezoidal dielectric load. It is constructed by stacking two same-shaped printed circuit boards with Rogers TMM3 substrate which is an anisotropic material. Since SIEW horn antenna has an horizontal electric field, it is important to clarify the differences of dielectric constant and loss tangent along different directions. As confirmed by the PCB manufacturer, the dielectric constant $\varepsilon_{rx} = \varepsilon_{ry} = 3.4$, $\varepsilon_{rz} = 3.45$ and loss tangent $tan\delta_x = tan\delta_y = tan\delta_z = 0.002$ are used. Except for the dielectric load, the top and bottom surfaces of the horn antenna are copper-plated, which act as top and bottom walls analogy to those of convention waveguide. Series of copper-plated through holes are perpendicularly drilled and are aligned along the wave propagating direction. All through holes have the same radius r = 0.5mm. In case that energy leaks through the gap between neighboring holes, the longitudinal spacing between two holes, namely the parameter d shown in Fig. 2.2, requires careful design to be small enough [17]. Essentially, since the failure of SIW to implement E-plane circuits is due to the lack of physical structure to support longitudinal current, copper strips are embedded in the middle between two circuit boards, where the peak value of sinusoidal current distribution of the TE_{10} mode as illustrated in [2] and shown in Fig. 2.3 [34]. A feeding network which includes an SMA adapter and a short SIEW section is employed, which is referred to as SIEW-to-SMA transition. The dimension of this transition is optimized by HFSS software. Moreover, for the sake of better impedance matching and return loss response, a trapezoidal dielectric load is etched in front of the horn aperture

whose optimum height is $L_l = 13.35$mm and width is $W_l = 7.308$mm as shown in Fig. 2.2. Parametric studies of both dimensions of dielectric load and SIEW-to-SMA transition will be presented in the next section. In order to excite only the horizontal polarized electric field as the fundamental mode while getting rid of disturbances from other high-order modes, the horizontal spacing between two copper plated through holes, namely the parameter b in Fig. 2.2, must be shorter than the thickness of the antenna $h = 5.1325$mm as shown in Fig. 2.1. Therefore, the top and bottom surfaces of the antenna become short walls by setting the parameter b to be 4.1mm. Consequently, the fundamental TE_{10} will be excited parallel to the circuit boards [2]. The proposed horn antenna was fabricated by the authors. The assembled single-element SIEW horn antenna is photographed in Fig. 2.4. The complete prototype (a) is constructed by stacking two printed circuit boards together, namely (b) and (c) in the photo. The shown surfaces of (b) and (c) are the middle layers of the circuits. The cutout of the substrate is for placement of the SMA inner conductor which should be soldered onto the T-shaped copper strip. After the middle copper strips are thinly tinned, parts (b) and (c) are stacked and clamped together in a reflow oven. Lastly, a piece of copper tape is used to cover the slot to prevent energy leakage.

2.2 Results and Discussions

In order to evaluate the transmission efficiency of the single-element antenna, the S-parameters are taken into account, which typically represents the relationship between different inputs and outputs of an electrical system. $|S_{11}|$, namely the reflection coefficient, represents how much energy is reflected back. A common requirement of this performance indicator is equal to or lower than -10dB, which means no more than 10% of energy is reflected. Consequently, in all our designs, the goal of S_{11} were set to be -10dB or lower. In the measurement, the antenna

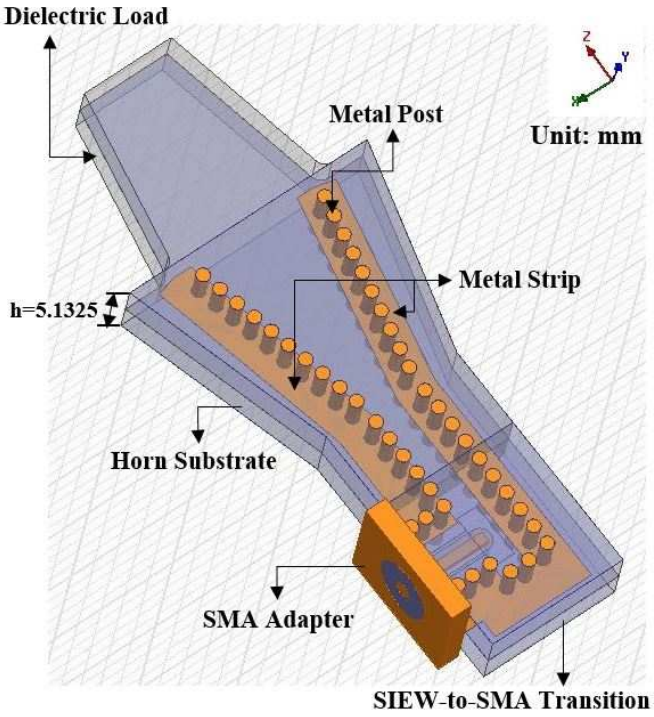

FIGURE 2.1: 3D geometry of the single-element SIEW horn antenna

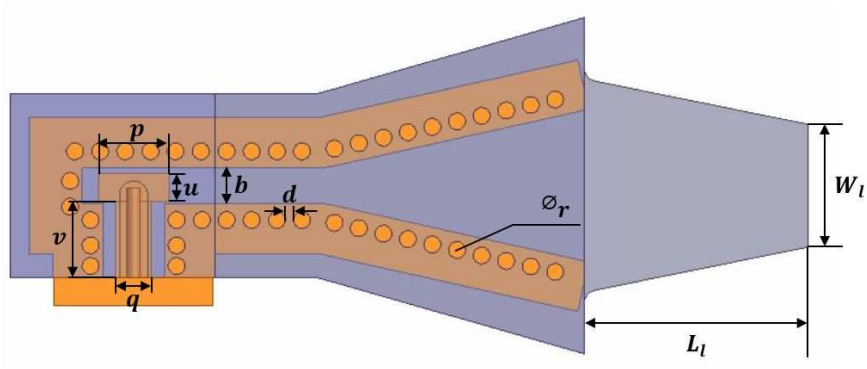

FIGURE 2.2: Cross-section view of the single-element SIEW horn antenna, $W_l = 7.308$mm, $L_l = 13.35$mm, $\Phi_r = 0.5$mm, $d = 0.5$mm, $b = 2.1$mm, $u = 1.68$mm, $p = 4.19$mm, $v = 4.56$mm, $q = 2.11$mm

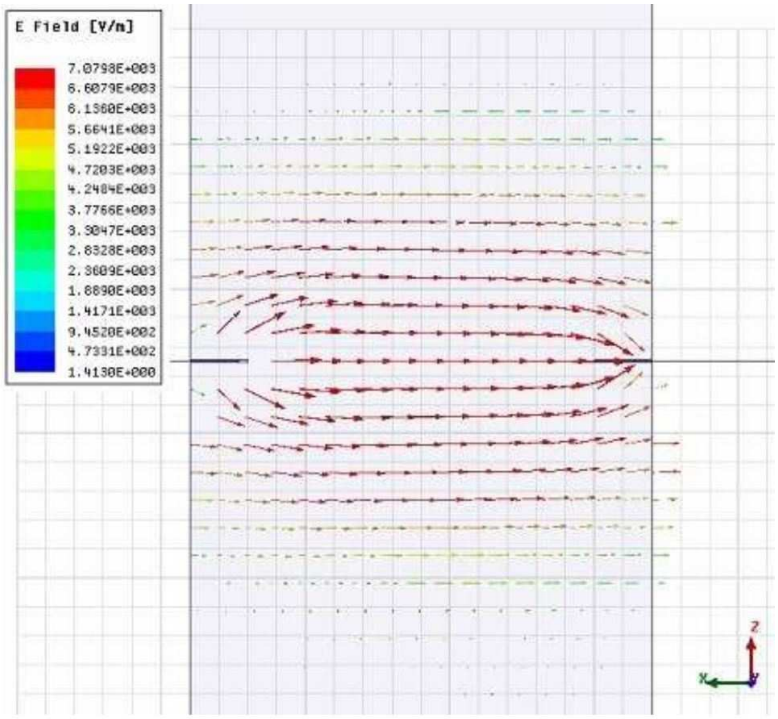

FIGURE 2.3: Electric field distribution of TE_{10} mode in a SIW circuit. Reprinted from "Concept of Substrate Integrated E-plane Waveguide and Waveguide Filter" by D. Huang, X. H. Wu and Q. Zhang, *International Workshop on Antenna Technology: Small Antennas, Innovative Structures, and Applications*, Cocoa Beach, FL, USA, Feb. 29 - Mar. 2, 2016.

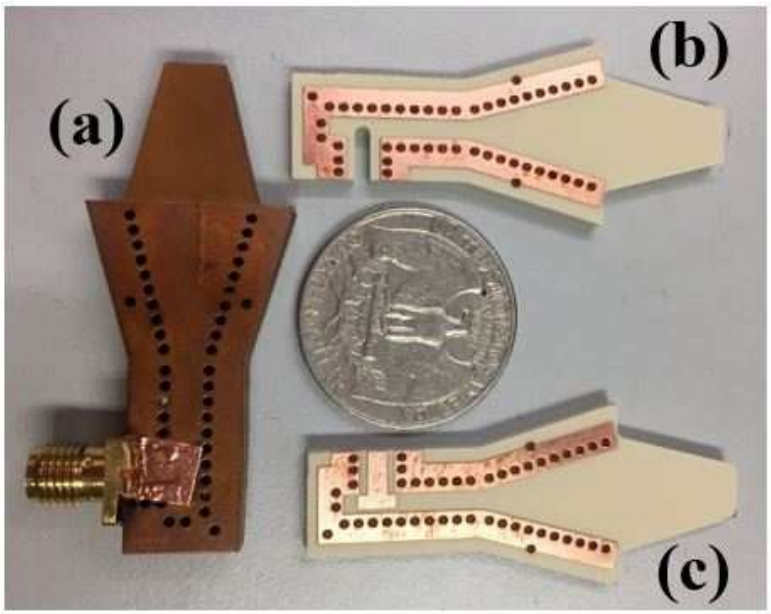

FIGURE 2.4: Prototype of single-element SIEW horn antenna

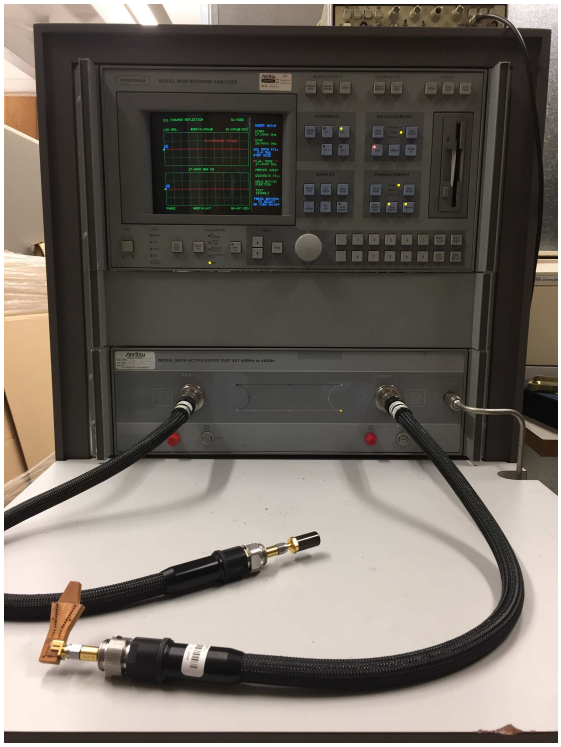

FIGURE 2.5: Environmental setup for measurement of $|S_{11}|$ of the single-element SIEW horn antenna

under test was connected to the vector network analyzer as shown in Fig. 2.5. The comparison of $|S_{11}|$ between results of simulation and measurement over an extended frequency band from 16GHz to 20GHz is depicted in Fig. 2.6. As expected, the reflection coefficient is controlled below -10dB over the entire working frequency band of 17-19GHz, namely 11% bandwidth is achieved.

As mentioned in the previous section, the dielectric load is supposed to minimize the reflections caused by the discontinuities between the substrate and free space at the aperture. In order to investigate effects introduced by the dielectric load, reflection coefficients and radiation patterns are compared between the SIEW horn antenna and the one without dielectric load respectively. As revealed in Fig. 2.7, the dielectric load contributes a much lower reflection coefficient within the working frequency band, namely the return loss is improved from 6dB to 10dB. In

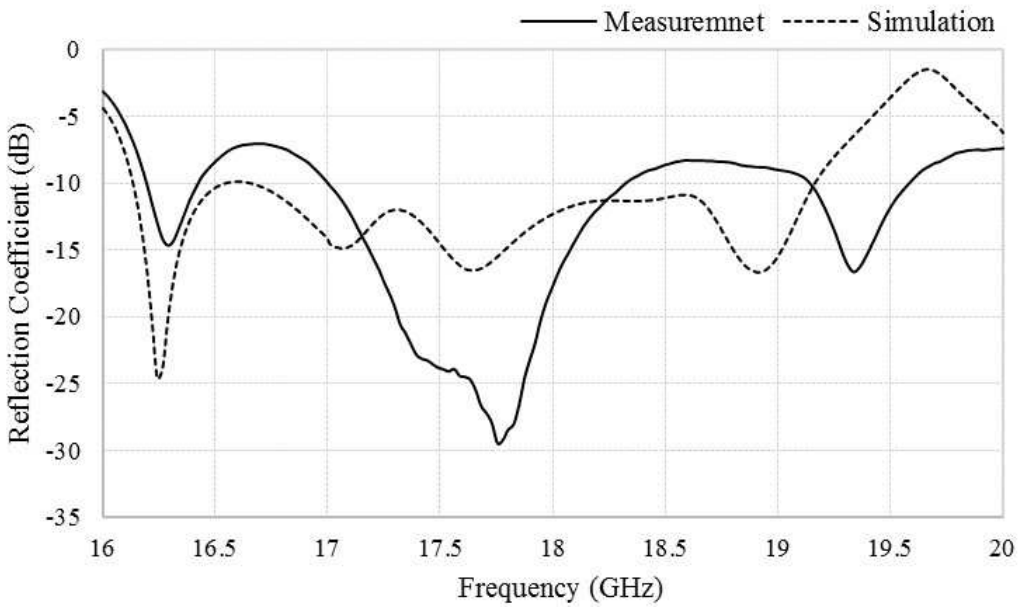

FIGURE 2.6: Simulated and measured $|S_{11}|$ of single-element SIEW horn antenna

other words, the dielectric load improves impedance matching by serving as the transition between the aperture and free space. After the optimization, reflections from the discontinuities can be cancelled out. Besides, Fig. 2.8 shows the radiation pattern of Co-polarization (Co-pol) in the E-plane. The radiation pattern is an important indicator of radiation performance. Detailed explanation will be presented on Co-polarization and Cross-polarization in Chapter 3. From Fig. 2.8, it is obvious to observe the dielectric load contributes as much as double gain at the center frequency 18GHz, namely the gain value is increased from 4.27dBi to 9.37dBi after the dielectric load is placed. Besides, the dielectric load is analogous to a lens to further focus the radiated energy in the wave propagating direction with a sharper beamwidth of 58° , when compared with beamwidth of 92° for the test antenna without the load. Conclusively, dielectric load is a significant benefit for improving radiating performance of the SIEW horn antenna.

As discussed above, since the dielectric load is such a determinant, further

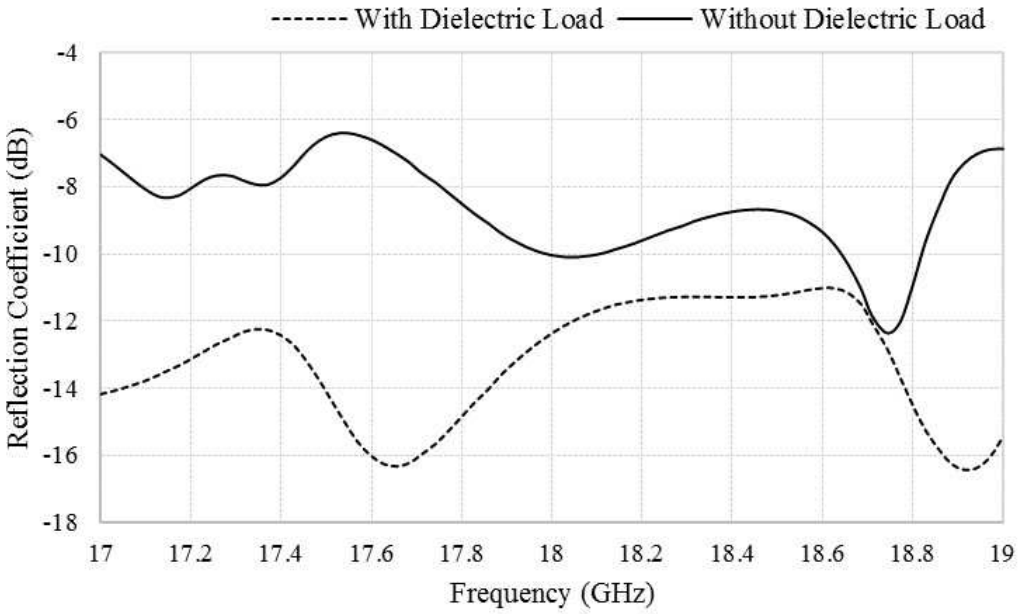

FIGURE 2.7: The effects of dielectric load on $|S_{11}|$

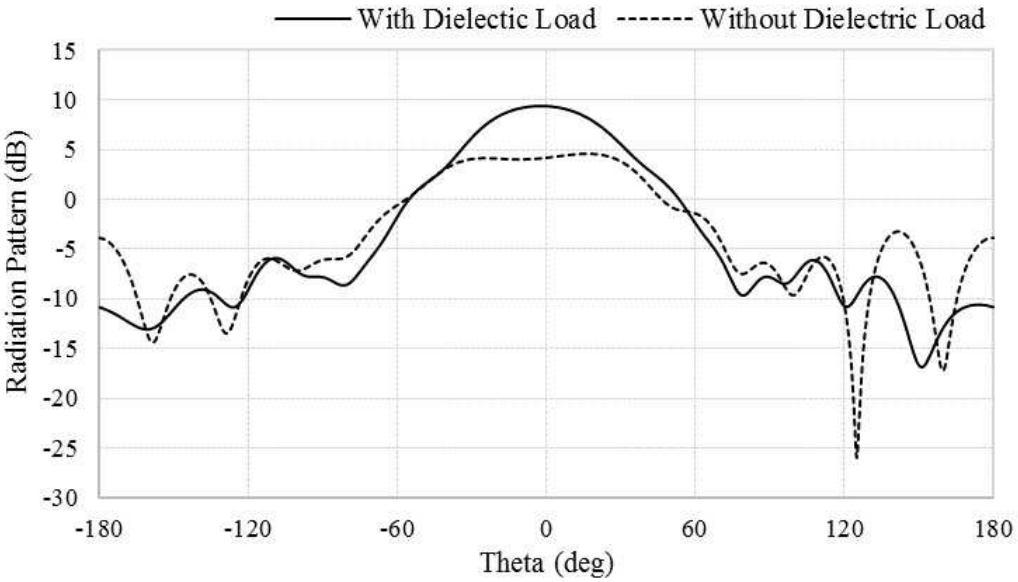

FIGURE 2.8: The effects of dielectric load on the radiation pattern of Co-pol at 18GHz

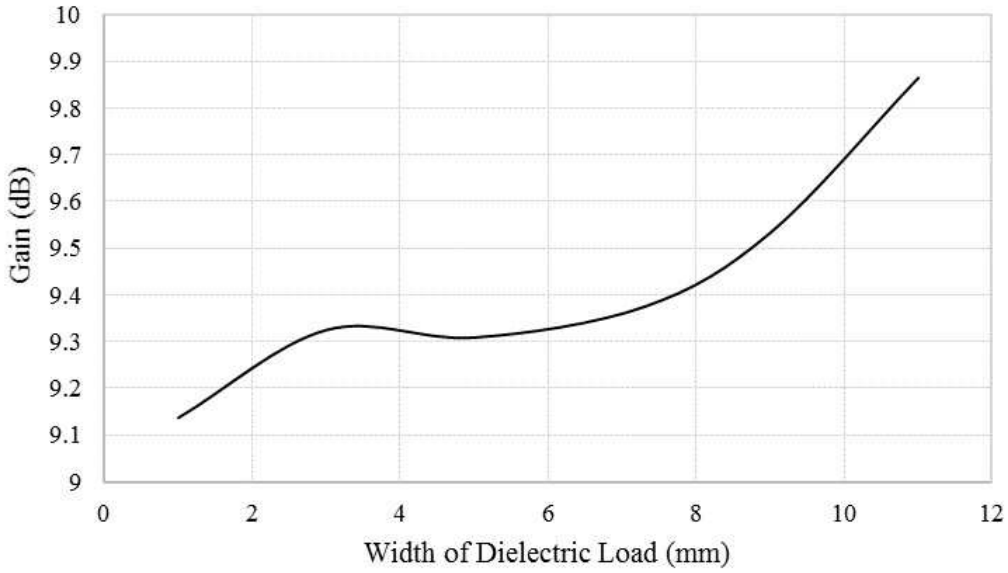

FIGURE 2.9: Gain comparison with different width values of dielectric load

studies have been taken on the size of the dielectric load towards antenna's performances. For example, two parameters are analyzed respectively, which are the W_l and L_l as shown Fig. 2.2. Maximal gain values at the center frequency of the working band and S-parameters are compared. In Fig. 2.9-Fig. 2.12, all other parameters are fixed when the values of W_l or L_l changes. It can be discovered that both parameters are sensitive to the gain values at the center frequency. Regarding to the S-parameters, when the value of W_l increases, the operating band of the test antenna moves towards higher frequency range. However, the S-parameters stably remain below -10dB when W_l exceeds its optimum value of 7.308mm, which indicates the W_l is no longer a sensitive parameter to the reflection coefficient. Similarly, a relatively high gain value and low reflection coefficient are obtained when the height of the load approaches its optimum value, namely 13.35mm. Notice that the optimum values for both parameters are all carried out with HFSS software.

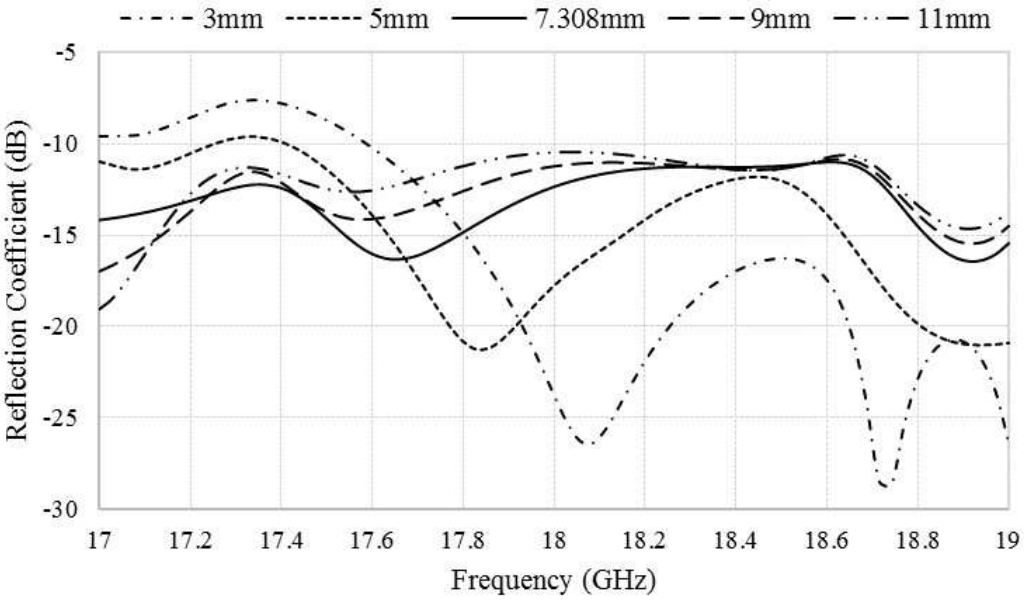

FIGURE 2.10: $|S_{11}|$ comparison with different width values of dielectric load

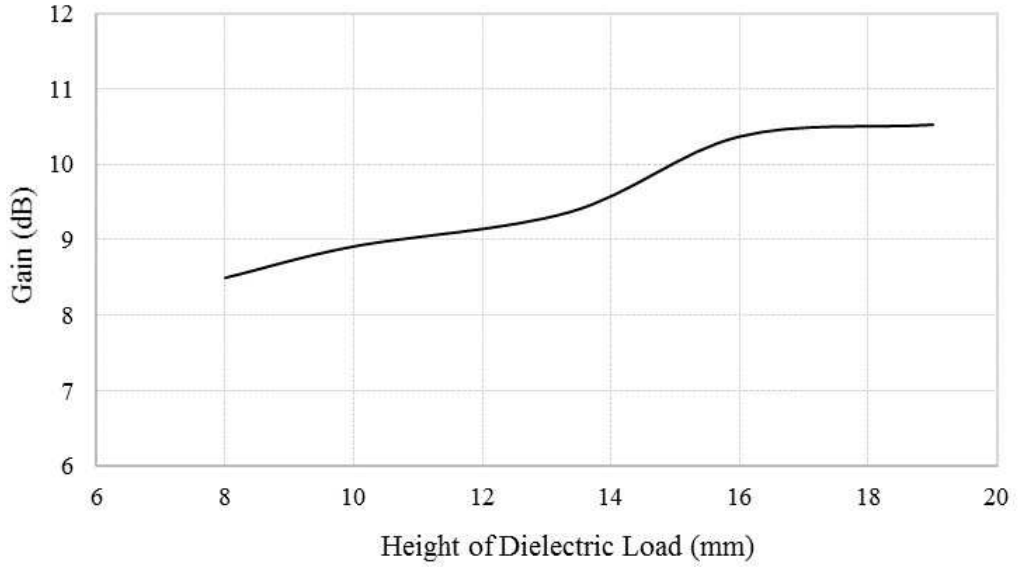

FIGURE 2.11: Gain comparison with different height values of dielectric load

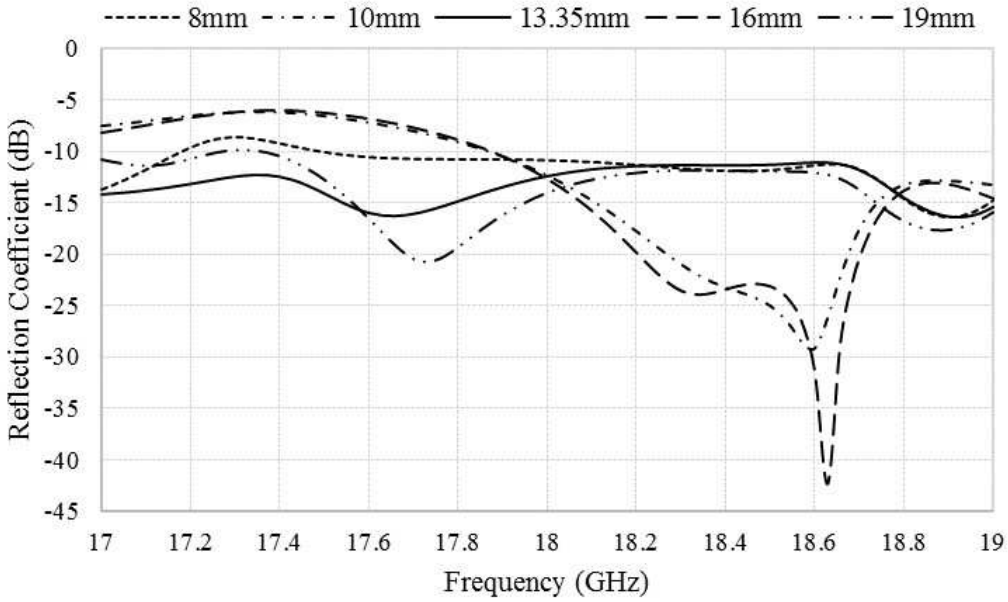

FIGURE 2.12: $|S_{11}|$ comparison with different height values of dielectric load

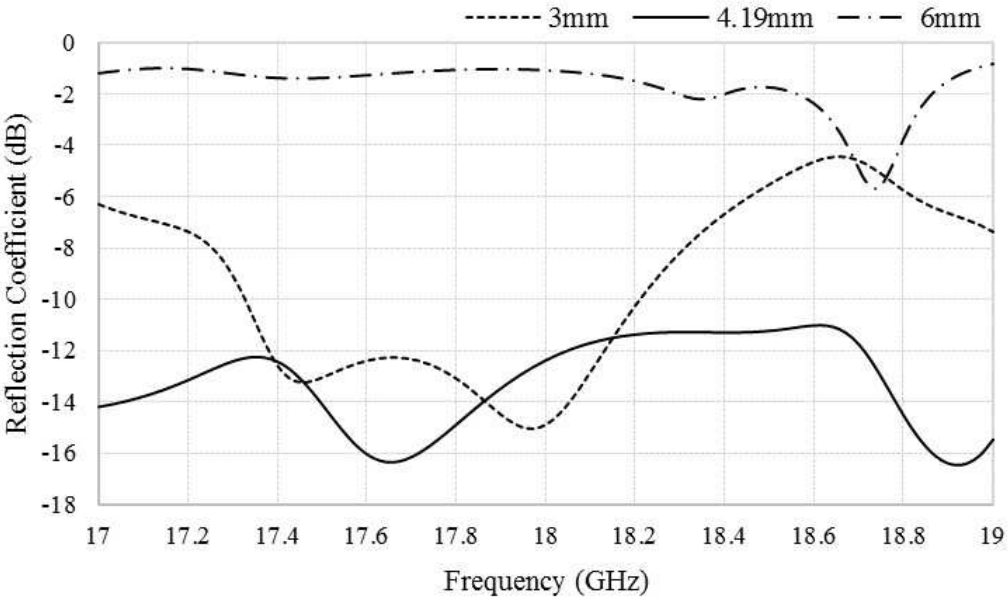

FIGURE 2.13: $|S_{11}|$ comparison with different values of p

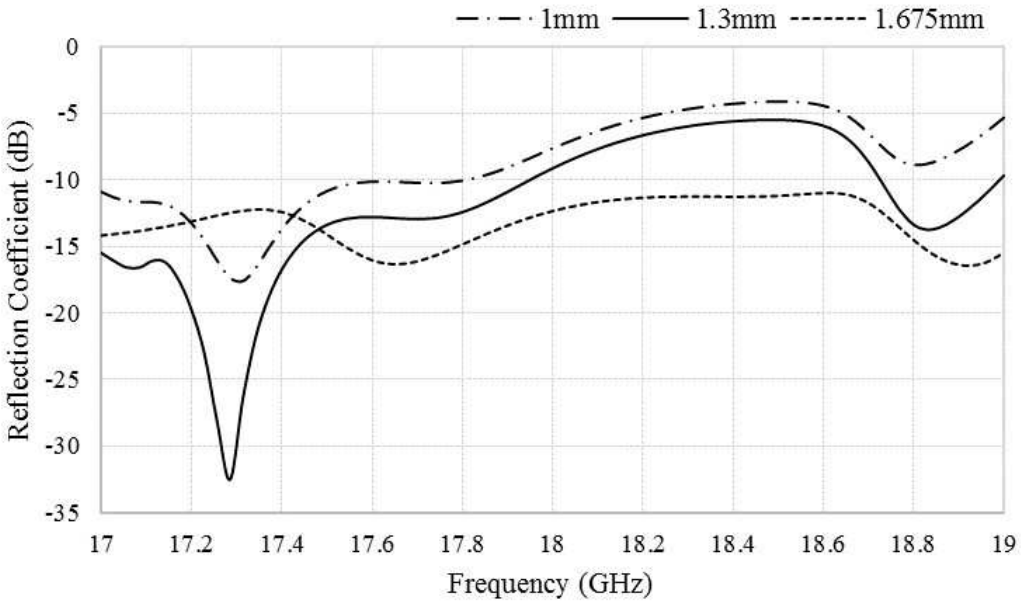

FIGURE 2.14: $|S_{11}|$ comparison with different values of u

As the frequent occurrences dance mismatch and energy loss, the SIEW-to-SMA transition also ought to be carefully designed. For example, two parameters, namely p and u as shown in Fig 2.2, have been analyzed to investigate how they affect the impedance matching of antenna. As illustrated in Fig. 2.13 and Fig. 2.14, the $|S_{11}|$ of the antenna were compared with different p and u values respectively. Obviously, it is shown that both p and u are very sensitive parameters for reflection coefficient. With the recommended values for p and u, namely p=4.187mm and u=1.3mm, the antenna generated more stable and better return loss response, where the $|S_{11}|$ is below -10dB across the working band.

3 SIEW Sectorial Horn Antenna Array

3.1 Antenna Array Geometry

As presented in the previous chapter, although either the transmitting or radiating performances of the single-element horn antenna is very good, however, the radiating level is still relative low if stronger power is required to be output. Antenna array, or phased array, can generate the accumulative power from its separate elements for radiating in the specific direction. By adjusting the spacing between elements, the radiation pattern of the array can also be adjusted.

In this chapter, a two-element SIEW horn antenna array excited by an SMA adapter is proposed to further enhance the antenna's performance. Its 3D geometry is depicted in Fig. 3.1. As shown in the figure, the proposed array consists of an SIEW-to-SMA transition, a two-way equal-split power divider, horn sections and dielectric loads. Series of metal-plated holes are aligned along the wave propagation direction. Particularly, the modified Y-shaped power divider is carefully designed to evenly distribute input power and provide more fluent paths for the flowing of longitudinal current. Fig. 3.2 provides the cross-section view of the antenna array. It is worth noting that a quarter-wavelength transformer is inserted between the power divider and the SIEW-to-SMA transition to match the transmission line impedance and eliminate reflections in this part. After the initial values of the dimension is setup based on the definition, the width W_{qt} and length L_{qt} of this quarter-wavelength transformer is further optimized by HFSS software for better results. In addition, the dimensions of the SIEW-to-SMA transition and two dielectric loads are based on that of single-element antenna, but also are further optimized in order to obtain optimum performances. Other dimensional data are labeled in Fig. 3.2. The total size of the whole circuit is $57 \times 32 \times 5.13 mm^3$ and

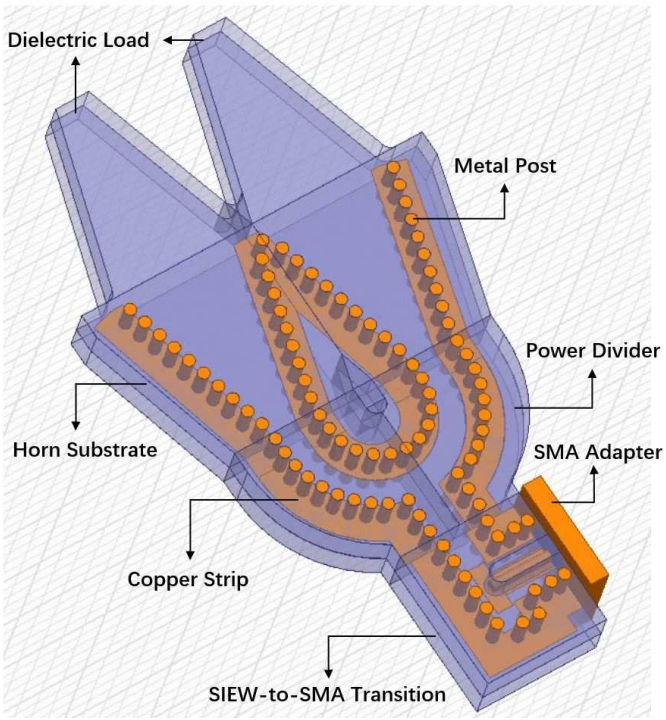

FIGURE 3.1: 3D geometry of SIEW horn antenna array

the photograph of the separate parts as well as fabricated antenna array prototype is shown in Fig. 3.3.

3.2 Results and Discussions

The transmitting and radiating performances of the antenna array have been both validated by simulated and measured results. The simulated and measured S-parameters are compared in Fig. 3.4. Good agreement has achieved especially at low frequency. The observed discrepancy between simulated and measured S-parameters can be attributed to the combined effects introduced by fabrication tolerance and anisotropic dielectric constant of the material [40]. With the limit on $|S_{11}|$ below -10dB, Fig. 3.4 shows that good return loss response over a wider frequency band was obtained from 16.3-19.9GHZ from measured results. This huge improvement is expected because the antenna is supposed to become more lossy

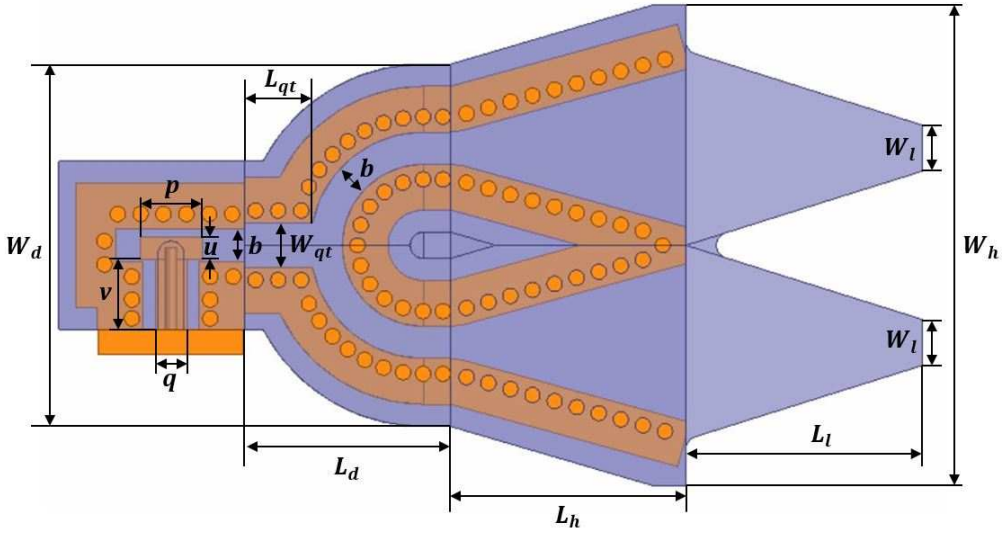

FIGURE 3.2: Cross-section view of the SIEW horn antenna array, W_l = 3.03mm, L_l = 15.46mm, W_h = 31.51mm, L_h = 15.41mm, W_d = 23.71mm, L_d = 13.50mm, b = 2.10mm, W_{qt} = 2.95mm, b=2.1mm L_{qt} = 4.43mm, p = 4.10mm, q = 2.10mm, u = 1.45mm, v = 4.61mm

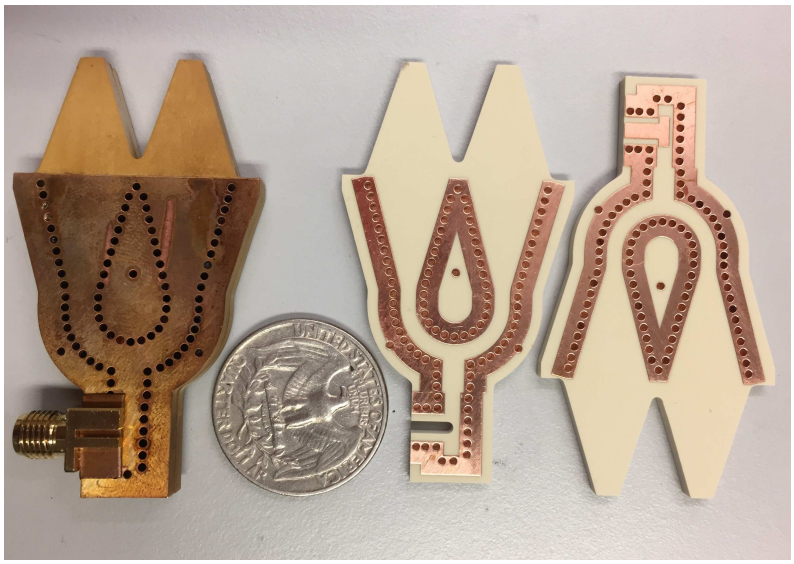

FIGURE 3.3: Separate parts and fabricated prototype of antenna array

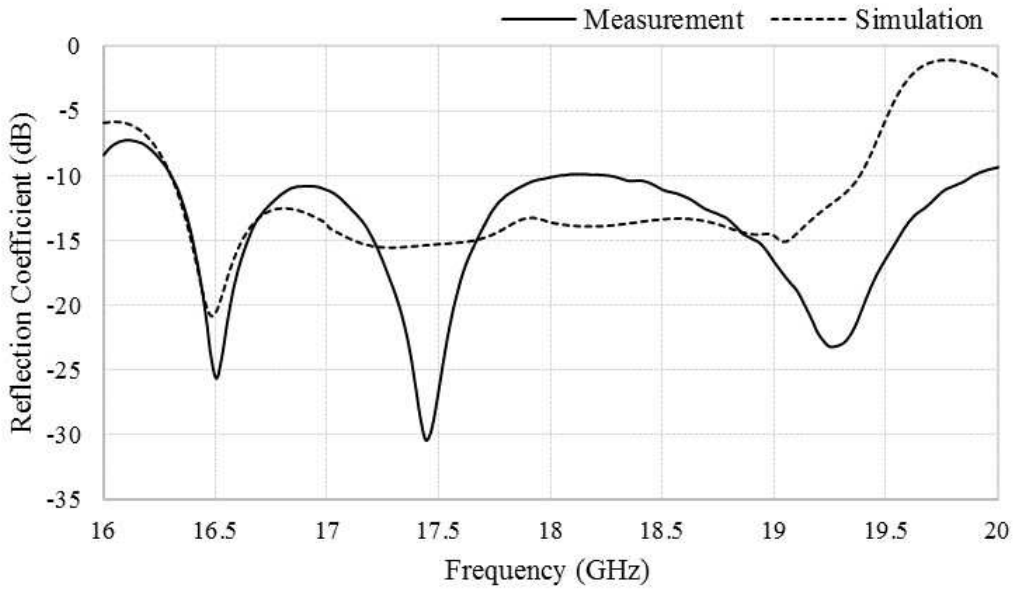

FIGURE 3.4: $|S_{11}|$ comparison within working frequency band

since the structure has been enlarged and complexity has been extended. In case that, instead of being radiated, the energy gets dissipated, the radiating behavior should also be considered. Gain values of the array in the band of 16-20GHz have also been measured and compared with the simulated ones. As shown in Fig. 3.5, a good agreement is achieved where the discrimination between the simulation and measurement is less than 1dB. The measured gain values especially show stability through the whole working band, which is an important characteristic especially for wideband communications and imaging systems [39]. As expected, when comparing with the single-element antenna, the array improved the gain value as much as 3dB , namely from 9.4dB to 12.4dB at 18GHz as shown, in Fig. 2.8 and Fig. 3.5. This result validates the proposed antenna array is able to improve radiating performance significantly.

Moreover, radiation patterns which indicate the radiation behavior in different directions are investigated. Typically, radiation patterns on two principle planes, E-plane and H-plane, are measured. E-plane is the plane as explained in 1, which

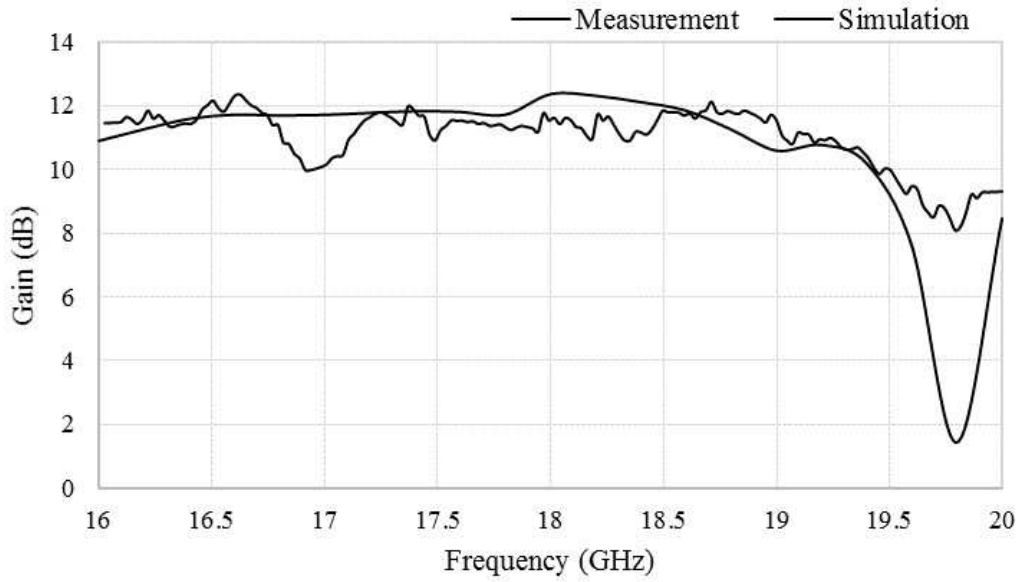

FIGURE 3.5: Gain of SIEW horn antenna array

is constructed by the vector of wave propagation direction and the vector of electric field. The electric field is polarized from the long wall to the other long wall of the waveguide circuit if the fundamental mode is excited. Similarly, H-plane is the plane of the vector of wave propagation direction and the vector of magnetic field. During the measurement, the antenna array was mounted on a servo motor on the receiving side, so that radiations patterns in E-plane can be measured when the E-plane of circuits is placed in the rotation plane of the servo motor. Since the H-plane is orthogonal to the E-plane, radiation patterns in H-plane can be measured by simply rotating the antenna circuit by 90 degrees, so that H-plane is in the rotation plane of the motor. On either plane, in terms of the antenna under test, two sets of patterns are taken into account. One is called Co-polarization (Co-pol), which is measured when the polarizations of transmitting antenna and test antenna are in the same direction. The other one is called Cross-polarization (X-pol), which is measured when the polarizations of both antenna are out-of-phase. In our measurements, radiation patterns were measured in three different

frequency points which are 17GHz, 18GHz and 19GHz respectively. The environment was built up for measuring as shown in Fig. 3.6. Both the transmitting side and receiving sides were placed in an anechoic chamber which is filled up with absorbing materials and were connected to the network analyzer to collect measured data. Meanwhile, a 10dBi standard gain horn antenna was fixed and used as the transmitter as photographed in Fig. 3.7. The initial position of the antenna array was facing back to the transmitter before the measurement started. Once the measurement begins, the servo motor carries the antenna array rotating horizontally for 360 degrees while the vector network analyzer scans and measures in the same time interval. As shown in Fig. 3.8 - Fig. 3.13, good agreements have been achieved between simulated and measured Co-pol patterns in both two principle planes, especially the main beams. Although the maximal values of Co-pol in two principle planes at the same frequency are supposed be equal, however due to the measurement tolerance and limitation of preventing noise in the testing environment, small differences occur. Anyhow, these are the best result can be achieved by the measurement, which is acceptable within the tolerance. As for the significant discrimination between the simulated and measured X-pol patterns, it is mainly attributed to the weakness of the transmitting power. Due to the limitation of equipment, although we have used a reflector to increase the transmitted power, however, the signal of X-pol is still too weak to be accruately measured. The noise cannot be sufficiently eliminated. Anyhow, the discrimination levels between the measured Co-pol and X-pol are from 15dB up to 20dB at all three frequency points, which are the best results we could get and it is still acceptable.

The symmetric Y-junction divider is designed to equally feed the power to two horn sections. It is connected to the SIEW-to-SMA transition to construct a closed

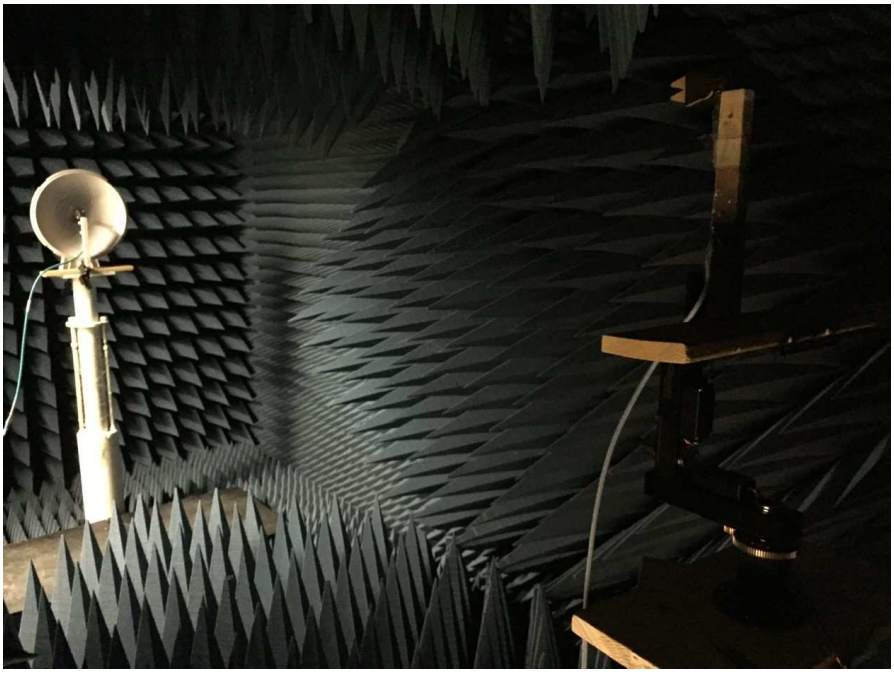

FIGURE 3.6: The photo of the environment setup of anechoic chamber

feeding network. As aforementioned, electric field is horizontally excited in SIEW circuits. By applying boundary conditions, it can be proved that longitudinal current will exist on side walls of antenna circuit to form a loop. As shown in Fig. 3.14, the equivalent circuit of an antenna array circuit consists of transmission lines ending with two loads in series. Since the gap b between middle strips remains constant, the characteristic impedance Z_o along the transmission line keeps the same. During the design process, the authors found that the power loss could hardly be eliminated by adjusting either the shape or size of the power divider. As a solution to improve impedance matching of the circuit, a quarter-wavelength transformer has been designed and inserted between the SIEW-to-SMA transition and power divider. The impedance of the transformer can be easily calculated to be $\sqrt{2}R$. Further detailly, the impedance along transmission lines can be described

FIGURE 3.7: The photo of the transmitting side

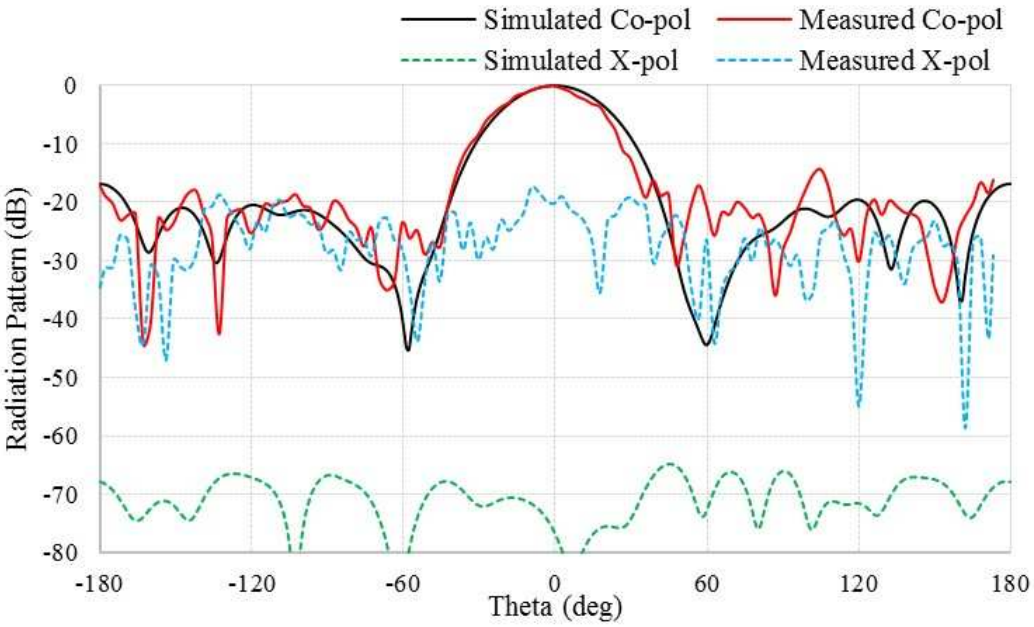

FIGURE 3.8: Radiation patterns in E-plane at 17GHz

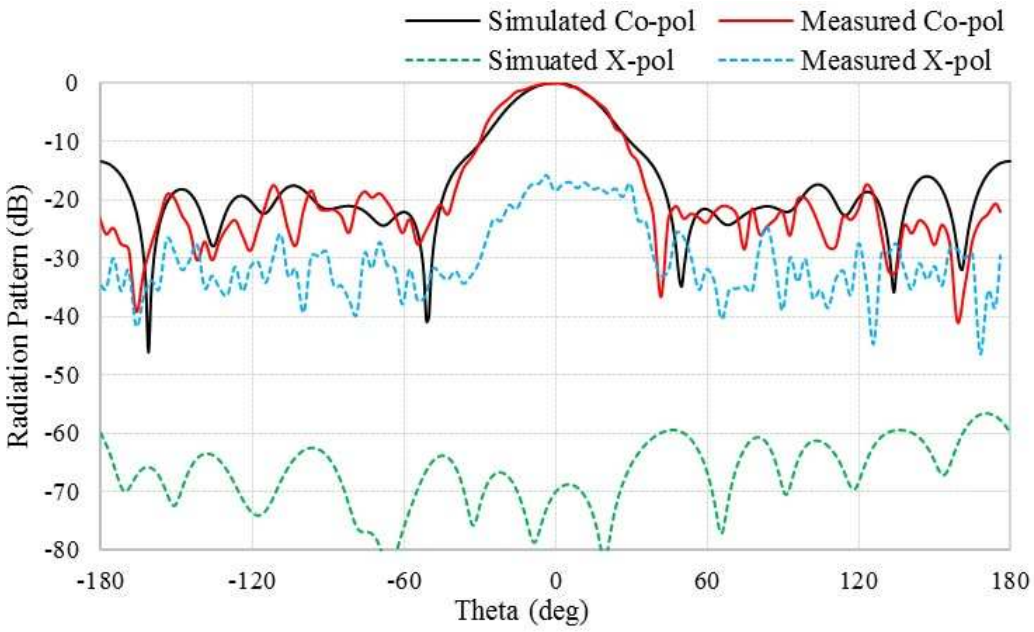

FIGURE 3.9: Radiation patterns in E-plane at 18GHz

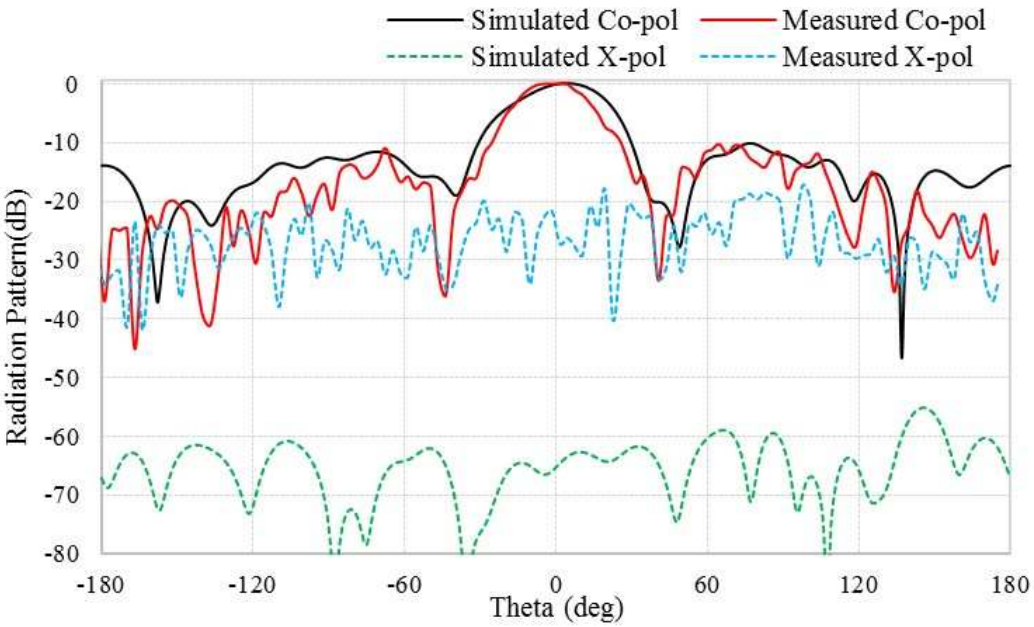

FIGURE 3.10: Radiation patterns in E-plane at 19GHz

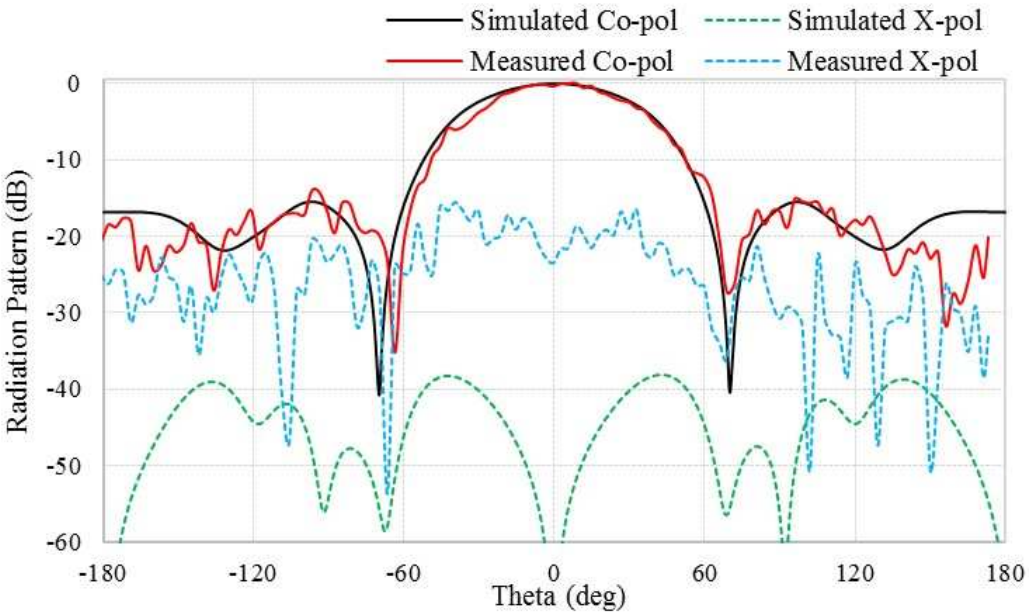

FIGURE 3.11: Radiation patterns in H-plane at 17GHz

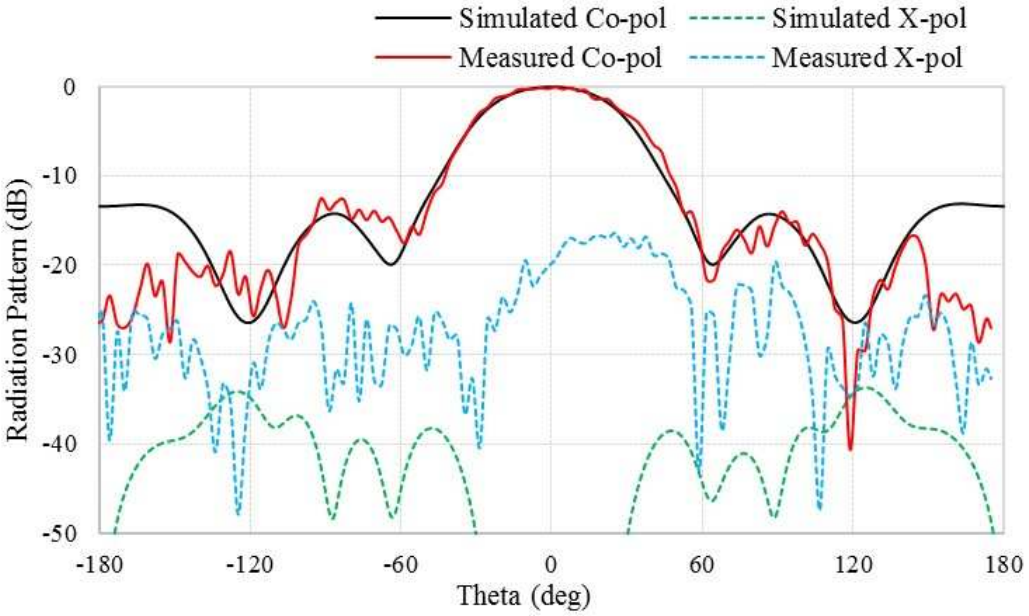

FIGURE 3.12: Radiation patterns in H-plane at 18GHz

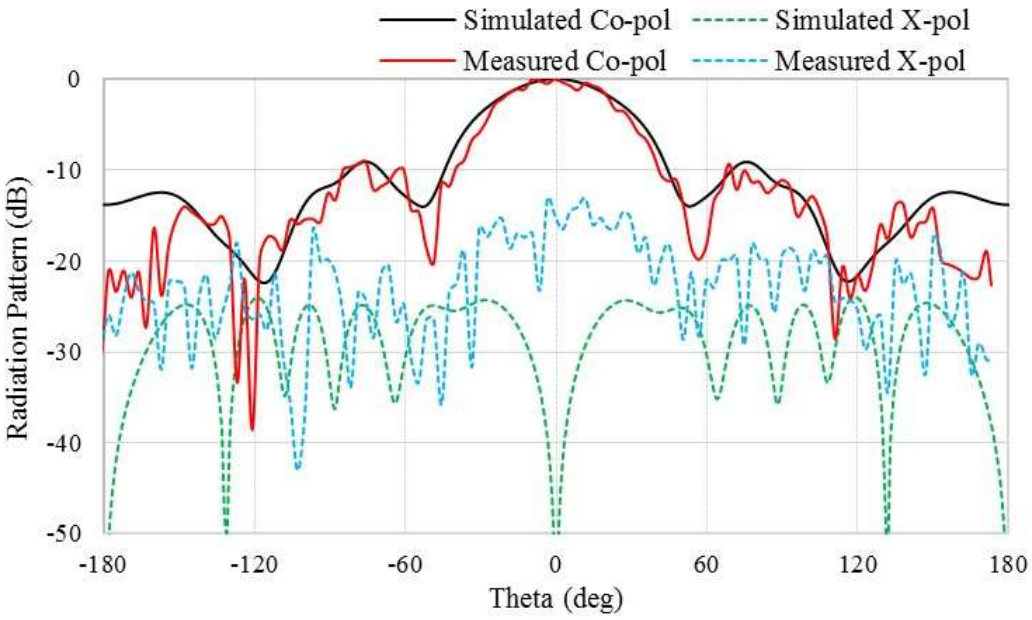

FIGURE 3.13: Radiation patterns in H-plane at 19GHz

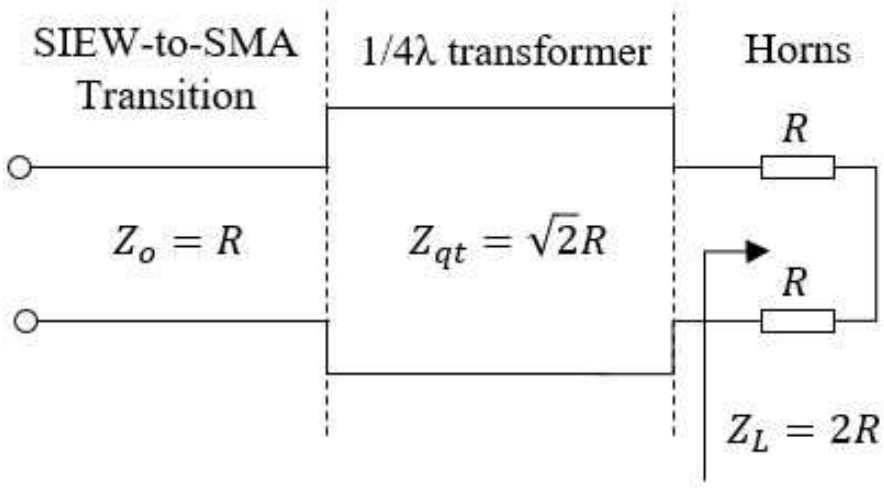

FIGURE 3.14: Equivalent circuit of antenna array

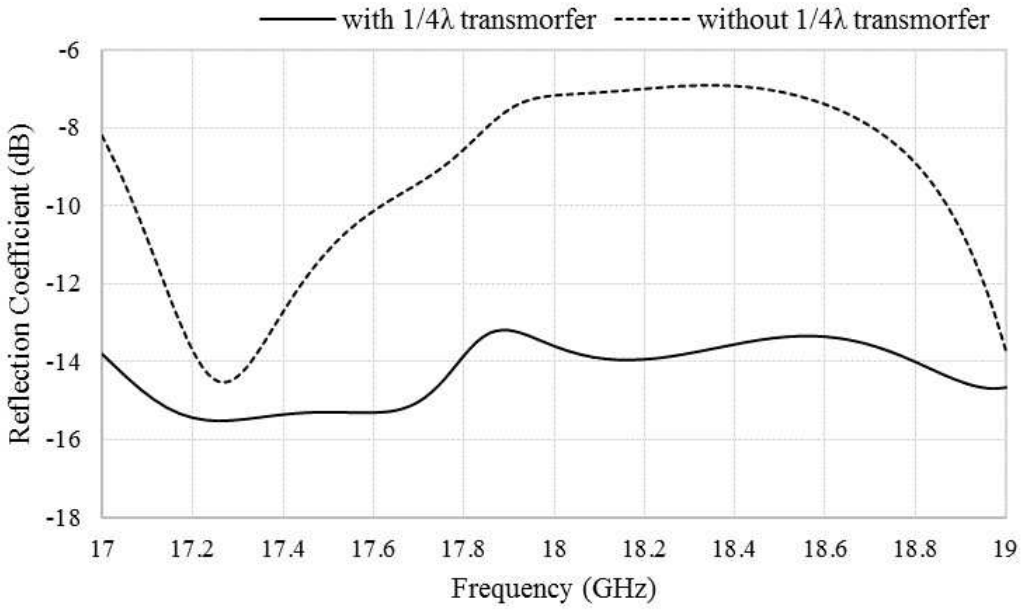

FIGURE 3.15: Effects of quarter-wavelength transformer on $|S_{11}|$ of array

as

$$R \propto \frac{E \times W}{H \times h} \tag{3.1}$$

It reveals that Z_o is only proportional to the width of circuit when other three parameters are fixed as in this case. Consequently, the theoretical value of width of the quarter-wavelength transformer W_{qt} should be $\sqrt{2}$ times of b. This relationship can be validated through measurements after optimization as labeled in Fig. 3.2. As for the length L_{qt}, guided quarter wavelength is initially assigned and further optimized by HFSS for better return loss response. As shown in Fig. 3.15, the quarter-wavelength transformer improves the impedance matching significantly over the entire working band.

4 Conclusion

Although conventional waveguide is a remarkable type of transmission lines with many advantages and have been widely used, however it is inadequate for integrated circuit and massive production. Substrate integrated waveguide (SIW) technique makes it possible to integrate planar waveguide on a simple printed circuit board (PCB) and it successfully implement all kinds of H-plane circuits. Whereas, it fails falling into E-plane circuits due to its intrinsic deficiency. To overcome this issue, a new technique substrate integrated E-plane waveguide (SIEW) technique was invented. Based on the concept of SIEW, a new type of horn antenna based on the substrate integrated E-plane waveguide (SIEW) technique is proposed and studied in this paper. The SIEW technique realizes the integration of conventional waveguide circuits on printed circuit boards (PCB) with more compact size and lower cost. By analyzing electromagnetic fields in both H-plane and E-plane types waveguide circuits, it is explored that only the vertical current on lateral walls exists in H-plane type circuits whereas additional longitudinal current along the propagation direction also exists in E-plane type circuits. This result explains the reason why the SIW fails implementing E-plane type circuits. As a solution, besides the metal-plated through holes, copper strips are embedded in the middle layer of the SIEW circuit. Consequently, vertical current can be guided by through holes while longitudinal current can flow along middle strips. Moreover, in order to improve the impedance matching, a dielectric load and SIEW-to-SMA transition are employed and carefully designed. All presented analytical results validate both of dielectric load and SIEW-to-SMA transition have been optimized to achieve the optimum performance of the antenna. Besides, a 1×2 antenna array is also designed to enhance the gain performance. A two-way

power divider is used as a feeding network company with an embedded quarter-wavelength impedance transformer in seeking of better return loss response. Both the simulated and measured results validate the antenna array has low return loss and high gain value over the working frequency band from 17-19GHz. The discrepancy between simulated and measured results are also discussed in this paper, which are mainly attributed to the anisotropic dielectric constant of the substrate and fabrication and measurement tolerances. Both prototypes are fabricated by stacking two same-shaped PCBs together, and bound in a reflow oven after the SMA adapter is soldered on. Conclusively, the SIEW technique is very potential in designing all kinds of E-plane integrated circuits.

References

[1] F. T. Ulaby, E. Michielssen, U. Ravaioli, *Fundamentals of Applied Electromagnetics*, 6th ed. Upper Saddle River, NJ: Prentice Hall, 2001.

[2] D. Pozar,*Microwave Engineering*, 2nd ed. New York, NY: Wiley, 1997.

[3] Y. Yang, C. Yuan, G. Cheng, and B. Qian, "Ku-Band Rectangular Waveguide Wide Side Dimension Adjustable Phase Shifter", *IEEE Transactions on Plasma Science*, vol. 43, no. 5, pp. 1666-1669, May 2015.

[4] D. Cai, J. Lu, Ch. Chen, Ch. Lee, Ch. Lin and T. Yen, "High Q-factor Microring Resonator Wrapped by the Curved Waveguide", *European Optical Society*, vol. 5, no. 1, 2015.

[5] V. Matvejev , C. Tandt , W. Ranson, J. Stiens, R. Vounckx and D Mangelings, "Integrated Waveguide Structure for Highly Sensitive THz Spectroscopy of Nano-liter Liquids in Capillary Tubes", *Progress in Electromagnetics Research*, vol. 121, pp. 89-101, 2011.

[6] M. Barbuto, F. Trotta, F. Bilotti and A. Toscano, "Filtering Chiral Particle for Rotating the Polarization State of Antennas and Waveguides Components", *IEEE Transactions on Antennas and Propagation*, vol. 65, pp. 1468-1471, 2017.

[7] M. Shafique and I. Robertson, "A Two-Stage Process for Laser Prototyping of Microwave Circuits in LTCC Technology", *Components Packaging and Manufacturing Technology IEEE Transactions*, vol. 5, pp. 723-730, 2015.

[8] D. Armand, H. Taniguchi, Y. Kadoya, T. Tanaka and K. Tanaka, "Terahertz Full Horn-Antenna Characterization", *Applied Physics Letters*, vol. 102, issue. 14, Apr. 2013.

[9] B. Damit, B. Bischoff, T. Phelps and Ch. Wu, "Filtration of Bioaerosols Using a Granular Metallic Filter with Micrometer-Sized Collectors", *Journal of Environmental Engineering*, vol. 140, issue. 12, Dec 2014.

[10] L. Delgado-Aparicio1, K. Tritz, T. Kramer, D. Stutman, M. Finkenthal, K. Hill1 and M. Bitter, "Soft X-ray Continuum Radiation Transmitted through Metallic Filters: An Analytical Approach to Fast Electron Temperature Measurements", *Review of Scientific Instruments*, vol. 81, issue. 10, Oct 2010.

[11] S. Wong, Sh. Feng, F. Deng, L. Zhu and Q. Chu, "A Quintuple-mode Wideband Bandpass Filter on Single Metallic Cavity With Perturbation Cylinders", *IEEE Microwave and Wireless Components Letters*, vol. 26, issue. 12, pp. 975-977, Dec 2016.

[12] Sh. Wang and T. Liu, "Four-Port Polarization and Topological Charge Controlled Directional Plasmonic Coupler", *IEEE Photonics Technology Letters*, vol. 28, pp. 2391-2394, 2016.

[13] X. Y. Zhang, Q. Guo, K. Wang, B. Hu and H. L. Zhang, "Compact Filtering Crossover Using Stub-Loaded Ring Resonator", *Microwave and Wireless Components Letters*, vol. 24, pp. 327-329, 2014, ISSN 1531-1309.

[14] L. Zhu, R. R. Mansour and M. Yu, "Compact Waveguide Dual-Band Filters and Diplexers", *IEEE Transactions on Microwave Theory and Techniques*, pp. 1-9, Jan 2017.

[15] W. Tu and Ch. Wu, "Design of Microstrip Low-PassBandpass Multiplexers Using Distributed Coupling Technique", *IEEE Transactions on Components Packaging and Manufacturing Technology*, vol. 5, issue. 4, pp. 1648-1655, Apr 2016.

[16] D. Deslandes and K. Wu, "Single-Substrate Integration Technique of Planar Circuits and Waveguide Filters", *IEEE Trans. Microwave Theory Tech.*, vol. 51, pp. 593-596, Feb. 2003.

[17] D. Deslandes and K. Wu, "Accurate Modeling, Wave Mechanisms, and Design Considerations of A Substrate Integrated Waveguide", *IEEE Trans. Microwave Theory Tech.*, vol. 54, pp. 2516-2526, Jun. 2006.

[18] W. Che, K. Deng, D. Wang, and Y. L. Chow, "Analytical Equivalence between Substrate-Integrated Waveguide and Rectangular Waveguide", *IET Microwaves, Antennas and Propagation*, vol. 2, no. 1, pp. 35-41, 2008.

[19] X. H. Wu, D. Huang and Q. Zhang, "Planar Substrate Integrated E-plane Waveguide (SIEW) Circuits", *IEEE Transactions on Microwave Theory and Techniques*, submitted in Apr, 2017.

[20] M. Bozzi, A. Georgiadis, and K. Wu, "Review of Substrate-Integrated Waveguide Circuits and Antennas", *IET Microwaves, Antennas and Propagation*, vol. 5, no. 8, pp. 909-920, 2011.

[21] X. Xu, R. G. Bosisio, and K. Wu, "A New Six-Port Junction Based on Substrate Integrated Waveguide Technology", *IEEE Trans. Microwave Theory Tech.*, vol. 53, pp. 2267-2273, Jul. 2005.

[22] F. Ruo, B. S. Izquierdo, P. R. Young, "Switchable Substrate Integrated Waveguide", *IEEE Microwave and Wireless Components Letters*, vol. 21, no. 4, pp. 194-196, Apr. 2011.

[23] F. Xu and K. Wu, "Guided-wave and Leakage Characteristics of Substrate Integrated Waveguide", *IEEE Transactions on Microwave Theory and Techniques*, vol. 53, no. 1, pp. 66-73, Jan, 2005.

[24] X. P. Chen and K. Wu, "Substrate Integrated Waveguide Filters: Design Techniques and Structure Innovations", *IEEE Microwave Magazine*, vol. 15, no. 6, pp. 121-133, Sep. 2014.

[25] P. Chu, W. Hong, K. Wang, H. Tang, Z. Hao, J. Chen and K. Wu, "Balanced Substrate Integrated Waveguide Filter", *IEEE Transactions on Microwave Theory and Techniques*, vol. 62, no. 4, pp. 824-831, Apr. 2014.

[26] Y. Wu, G. Li, W. Yang and T. Mou, "A Novel Dual-Band SIW Filter with High Selectivity", *Progress In Electromagnetics Research Letters*, vol. 60, pp. 81-88, 2016.

[27] A. Ali, H. Aubert, N. Fonseca and F. Coccetti, "Wideband Two-Layer SIW Coupler: Design and Experiment", *Electronics Letters*, vol. 45, no. 13, pp. 687-689, Jun 2009.

[28] A. Nasri, H. Zairi, and A. Gharsallah, "Single Balanced Mixer Using Substrate Integrated Waveguide (SIW) 90 Degree Coupler", *International Journal of Engineering and Technology*, vol. 8, issue. 1, pp. 61-64, Jan 2016.

[29] H. Oraizi, "Design of Miniaturized Planar SIW Diplexers Uing Dual-mode Resonators", *Letters on Progress in Electromagnetics Research*, vol. 54, pp. 129-135, 2015.

[30] M. Chen, H. Cheng, P. Chou and Ch. Chang, "W-band T-Junction and Bifurcated Substrate Integrated Waveguide Diplexers", *IEEE Conference*, pp. 1-2, Nov 2015.

[31] H. D. Wang, D. Fang, B. Zhang and W. Chen, "Dielectric Loaded Substrate Integrated Waveguide (SIW) H-plane Horn Antennas", *IEEE Trans. Antennas Propagat.*, vol. 58, no. 3, pp. 640-647, 2010.

[32] M. Esqulus-Morote, B. Funchs, J. Zrcher and J. R. Mosig, "Novel Thin and Compact H-Plane SIW Horn Antenna", *IEEE Transactions on Antennas and Propagation*, vol. 61, no. 6, Jun. 2013.

[33] N. Bayat-Makou, M. S. Sorkherizi and A. A. Kishk, "Substrate Integrated Horn Antenna Loaded with Open Parallel Transitions", *IEEE Antennas and Wireless Propagation Letters*, vol. PP, no. 99, pp.1-1.

[34] D. Huang, X. H. Wu and Q. Zhang, "Concept of Substrate Integrated E-plane Waveguide and Waveguide Filter", *International Workshop on Antenna Technology: Small Antennas, Innovative Structures, and Applications*, Cocoa Beach, FL, USA, Feb. 29 - Mar. 2, 2016.

[35] Z. Gu, D. Huang, X. H. Wu and Q. Zhang, "Substrate Integrated E-plane Horn Antenna", *IEEE International Symposium on Antennas and Propagation*, Fajardo, Puerto Rico, Jun. 26 - Jul. 1, 2016.

[36] Y. J. Cheng, W. Hong and K. Wu, "94 GHz Substrate Integrated Monopulse Antenna Array", *IEEE Transactions on Antennas and Propagation*, vol. 60, no. 1, pp. 121-129, Jan. 2012.

[37] Z. Chen, Y. Zhang, A. Bisognin, D. Titz, F. Ferrero and C. Luxey, "A 94-GHz Dual-Polarized Microstrip Mesh Array Antenna in LTCC Technology", *IEEE Antennas and Wireless Propagation Letters*, vol. 15, pp. 634-637, 2016, ISSN 1536-1225.

[38] X. Zou, C. Tong and D. Yu, "Y-junction Power Divider Based on Substrate Integrated Waveguide", *Electronics Letters*, vol. 47, no. 25, pp. 1375-1376, Dec. 2011.

[39] Y. Cheng, Y. Guo and Z. Lin, "W-Band Large-Scale High-Gain Planar Integrated Antenna Array", *IEEE Transactions on Antennas and Propagation*, vol. 62, no. 6, pp. 3370-3373, Jun. 2014.

[40] N. Ghassemi, K. Wu, S. Claude, X. Zhang and J. Bornemann, "Low-Cost and High-Effcient W-band Substrate Integrated Waveguide Antenna Array Made of Printed Circuit Board Process", *IEEE Transactions on Antennas and Propagation*, vol. 60, no. 3, pp. 1648-1653, Mar. 2012.